A&A 446, 459–470 (2006)
DOI: 10.1051/0004-6361:20053893

Astronomy & Astrophysics

X-ray spectral survey with XMM–Newton of a complete sample of nearby Seyfert galaxies⋆

M. Cappi[1], F. Panessa[2], L. Bassani[1], M. Dadina[1], G. DiCocco[1], A. Comastri[3], R. Della Ceca[4], A. V. Filippenko[5], F. Gianotti[1], L. C. Ho[6], G. Malaguti[1], J. S. Mulchaey[6], G. G. C. Palumbo[7], E. Piconcelli[8], W. L. W. Sargent[9], J. Stephen[1], M. Trifoglio[1], and K. A. Weaver[10]

[1] INAF-IASF Sezione di Bologna, via Gobetti 101, 40129 Bologna, Italy
e-mail: cappi@bo.iasf.cnr.it
[2] Instituto de Fisica de Cantabria (CSIC-UC), Avda de los Castros, 39005 Santander, Spain
[3] INAF- Osservatorio Astronomico di Bologna, via Ranzani 1, 40127 Bologna, Italy
[4] INAF- Osservatorio Astronomico di Brera, via Brera 28, 20121 Milano, Italy
[5] Department of Astronomy, University of California, Berkeley, CA 94720-3411, USA
[6] Carnegie Observatories, 813 Santa Barbara Street, Pasadena, CA 91101, USA
[7] Dipartimento di Astronomia, Universita' degli Studi di Bologna, via Ranzani 1, 40127 Bologna, Italy
[8] XMM–Newton Science Operation Center/RSSD-ESA, Apartado 50727, 28080 Madrid, Spain
[9] Department of Astronomy, California Institute of Technology, Pasadena, CA 91125, USA
[10] Laboratory for High Energy Astrophysics, NASA's Goddard Space Flight Center, Greenbelt, MD 20771, USA

Received 23 July 2005 / Accepted 28 September 2005

ABSTRACT

Results obtained from an X-ray spectral survey of nearby Seyfert galaxies using *XMM–Newton* are reported. The sample was optically selected, well defined, complete in B magnitude, and distance limited: it consists of the nearest ($D \lesssim 22$ Mpc) 27 Seyfert galaxies (9 of type 1, 18 of type 2) taken from the Ho et al. (1997a, ApJS, 112, 315) sample. This is one of the largest atlases of hard X-ray spectra of low-luminosity active galaxies ever assembled. All nuclear sources except two Seyfert 2s are detected between 2 and 10 keV, half for the first time ever, and average spectra are obtained for all of them. Nuclear luminosities reach values down to 10^{38} erg s^{-1}. The shape of the distribution of X-ray parameters is affected by the presence of Compton-thick objects ($\gtrsim$30% among type 2s). The latter have been identified either directly from their intense FeK line and flat X-ray spectra, or indirectly with flux diagnostic diagrams which use isotropic indicators. After taking into account these highly absorbed sources, we find that (i) the intrinsic X-ray spectral properties (i.e., spectral shapes and luminosities above 2 keV) are consistent between type 1 and type 2 Seyferts, as expected from "unified models"; (ii) Seyfert galaxies as a whole are distributed fairly continuously over the entire range of $N_{\rm H}$, between 10^{20} and 10^{25} cm^{-2}; and (iii) while Seyfert 1s tend to have lower $N_{\rm H}$ and Seyfert 2s tend to have the highest, we find 30% and 10% exceptions, respectively. Overall the sample is of sufficient quality to well represent the average intrinsic X-ray spectral properties of nearby active galactic nuclei, including a proper estimate of the distribution of their absorbing columns. Finally, we conclude that, with the exception of a few cases, the present study agrees with predictions of unified models of Seyfert galaxies, and extends their validity down to very low luminosities.

Key words. X-rays: galaxies – galaxies: Seyfert – glaxies: active

1. Introduction

X-ray studies are crucial in understanding active galactic nuclei (AGNs) because of the unambiguous association of high-energy emission with genuine nuclear activity and the important diagnostics provided in this band for studying accretion mechanisms.

Hard X-ray selected samples of nearby Seyfert galaxies available from studies with *GINGA*, *ASCA*, and *BeppoSAX* (Awaki et al. 1991; Smith & Done 1996; Turner et al. 1997a,b, 1998; Bassani et al. 1999) have been used to (successfully) verify the validity of unified models of AGNs. These models try to explain the observed differences between broad (Seyfert 1-like) and narrow (Seyfert 2-like) emission-line active galaxies by invoking obscuration (from an optically and geometrically thick torus) and viewing-angle effects rather than intrinsic physical differences (Antonucci 1993). The largest compilations of hard X-ray spectra available to date have, however, been severely biased toward the most X-ray luminous, and less absorbed, AGNs. Studies by Maiolino et al. (1998) and

⋆ Appendices A and B are only available in electronic form at http://www.edpsciences.org

Risaliti et al. (1999) reduced these selection effects by applying a careful analysis for a sample of type 2 Seyferts limited in [O III] flux. They discovered the existence of a large fraction ($\gtrsim$50–60%) of highly obscured AGNs at low redshifts, a result which confirms the bias against heavily obscured systems affecting previous surveys.

With the advent of new sensitive X-ray telescopes, there is now hope of probing the applicability of standard accretion-disk theories down to very low nuclear luminosities and, possibly, for AGNs with smaller black hole masses. Recent studies performed with the last generation X-ray observatories have extended the X-ray spectral analysis down to lower luminosities, sometimes also comparing Seyferts with LINERs (Heckman 1980) and/or H II-starburst galaxies (e.g., Terashima et al. 2002; Georgantopoulos et al. 2002). Snapshot surveys with *Chandra* have been able to detect for the first time point-like nuclear sources in increasingly larger samples of nearby galaxies at very low luminosities (down to less than 10^{38} erg s^{-1}; Ho et al. 2001; Terashima & Wilson 2003). Such studies seem to suggest that the standard unified model may not hold down to such low luminosities because low luminosity sources have X-ray luminosities a factor of 10 below the $L_{\rm X} - L_{\rm H_\alpha}$ relation for more luminous AGNs.

Moreover, deep *Chandra* and *XMM-Newton* surveys indicate that the bulk of the X-ray background (XRB) originates at relatively low redshift ($z \approx 1$) and is due to a combination of unobscured (type 1) and obscured (type 2) Seyfert galaxies (Hasinger et al. 2001; Mateos et al. 2005) as expected by synthesis models based on AGN unified schemes (Setti & Woltjer 1989; Comastri et al. 1995; Gilli et al. 2001). Given that a large fraction of the XRB is due to relativly low luminosity sources (lower than 10^{44} erg s^{-1}) and that the $N_{\rm H}$ distribution is essentially a free parameter in AGN models, a precise knowledge of the true column density distribution of nearby Seyfert galaxies, especially in the low luminosity regime, is essential.

With the aim of sorting out some of the questions raised by the above arguments, we decided to perform an X-ray survey on a well defined, bias-free sample of Seyfert galaxies. The present sample contains the 27 nearest Seyfert galaxies (with $D < 22$ Mpc) of the sample presented by Ho et al. (1997, HFS97a). The X-ray survey reported here are the results obtained using the EPIC CCDs on-board *XMM-Newton*. This survey is part of a larger program (Panessa 2004) aimed at characterizing and understanding the multi-wavelength properties of all 60 sources with a Seyfert classification taken from HFS97a.

Compared to previous studies, the strength of using *XMM–Newton* rests on two main facts: its high throughput (especially at energy $E > 2$ keV) allows a search for spectral components with absorption columns up to $N_{\rm H} \approx 10^{22}$–$10^{24}$ cm^{-2}, and its spatial resolution (half-power radius $\sim$7″) minimizes any strong contamination from off-nuclear sources to the soft ($E < 2$ keV) and/or hard ($E \gtrsim 2$ keV) energy band.

A description of the sample, observations, and data reduction can be found in Sect. 2. Section 3 summarizes the spatial and timing analysis. Spectra are shown in Sect. 4 together with a summary of the source spectral parameters in tabular form. Spectral properties are detailed in Sect. 5, and the results and conclusions are summarized in Sect. 6. A discussion of the spectral properties of each individual object is deferred to the Appendix.

2. The sample, observations, and data reduction

The sample studied in this paper is drawn from 52 nearby Seyfert galaxies given in HFS97a (see also Ho & Ulvestad 2001, HU01 hereinafter). Originally derived from the Palomar optical spectroscopic survey of nearby galaxies[1] (Filippenko & Sargent 1985; Ho et al. 1995), this sample has the advantage of having uniform and high-quality data that allowed the Seyfert classifications to be determined with well-defined and objective criteria (HFS97a). It is among the most complete and least biased samples of Seyfert galaxies available to date (see Appendix in HU01).

For the purpose of this study, we choose the nearest AGNs in the HFS97a sample – the 30 Seyfert galaxies which are within a distance of 22 Mpc. Three of these have been excluded from the present analysis: the Seyfert 2 galaxy NGC 185 for having line intensity ratios probably produced by stellar processes rather than an AGN (HU01), the Seyfert 1.9 galaxy NGC 3982 for lack of available *XMM–Newton* data at the time of writing, and the Seyfert 1.9 galaxy NGC 4168 which no longer meets the distance criterion[2].

Two objects, NGC 4395 and NGC 4579, have been classified by Ho et al. (1997b) as S1.8 and S1.9/L1.9, respectively. However, here we reclassify these sources as type 1.5 objects. A broad component is indeed clearly present in a number of optical (Filippenko & Sargent 1989) and ultraviolet (Filippenko et al. 1993) emission lines of NGC 4395. In addition, the UV spectrum of NGC 4395 resembles those of Seyfert 1s (Schmitt & Kinney 1996). Extremely broad permitted lines have been detected in NGC 4579. The *FWHM* of C IV is over 6000 km s^{-1} in this object, meeting the criteria of a standard broad-line region (BLR), although it is fainter than the BLR in bright Seyfert nuclei (Barth et al. 1996, 2001). In addition, two objects (NGC 4639, NGC 4051) have been reclassified as Seyfert 1.5 (from 1.0 and 1.2, respectively); they have prominent narrow-line regions (NLRs) along with their BLRs.

The final sample consists of 27 Seyfert galaxies which include 9 type 1s (specifically type 1.5) and 18 type 2 s. (Here, the "type 2" category is defined to include type 1.9 as well, because the broad Hα line is very hard to detect in spectra having low signal-to-noise ratios; moreover, such nuclei may be largely obscured, as are many of the "pure" Seyfert 2s.) The sample properties are listed in Table 1.

A log of all *XMM–Newton* observations is shown in Table 2. Seventeen objects were observed as part of the EPIC Guaranteed Time observation program with exposure time

[1] The Palomar survey presented in Ho et al. (1995) includes high-quality spectra of 486 bright ($B_T \lesssim 12.5$ mag), northern ($\delta > 0°$) galaxies for which a comprehensive, homogeneous catalog of spectral classifications have been obtained (HFS97a). The Palomar survey is complete to $B_T = 12.0$ mag and 80% complete to $B_T = 12.5$ mag (Sandage et al. 1979).

[2] Its original distance measurement ($D = 16.8$ Mpc; Tully 1988) has been updated recently to $D = 31.7$ Mpc (Caldwell et al. 2003).

Table 1. The complete, distance-limited sample of Seyfert galaxies.

Galaxy name (1)	Other name (2)	Seyfert type (3)	Hubble type (4)	Distance (Mpc) (5)	B_T (mag) (6)	RA (J2000) (7)	Dec (J2000) (8)
NGC 676		S2:	S0/a: spin	19.5	10.50	01 48 57.4	+05 54 25.7
NGC 1058		S2	Sc	9.1	11.82	02 43 30.2	+37 20 27.2
NGC 1068		S1.9	Sb	14.4	9.61	02 42 40.7	-00 00 47.6
NGC 2685	Arp336	S2/T2:	SB0+ pec	16.2	12.12	08 55 34.8	+58 44 01.6
NGC 3031	M81	S1.5/L1.5	Sab	3.5[a]	7.89	09 55 33.2	+69 03 55.0
NGC 3079		S2	SBc spin	17.3[b]	11.54	10 01 58.5	+55 40 50.1
NGC 3185		S2:	SB0/a	21.3	12.99	10 17 38.7	+21 41 17.2
NGC 3227	Arp94	S1.5	SABa pec	20.6	11.10	10 23 30.6	+19 51 53.9
NGC 3486		S2	SABc	7.4	11.05	11 00 24.1	+28 58 31.6
NGC 3941		S2:	SB0	12.2[c]	11.25	11 52 55.4	+36 59 10.5
NGC 4051		S1.5*	SABbc	17.0	10.83	12 03 09.6	+44 31 52.8
NGC 4138		S1.9	S0+	13.8[c]	12.16	12 09 29.9	+43 41 06.0
NGC 4151		S1.5	SABab:	20.3	11.50	12 10 32.6	+39 24 20.6
NGC 4258	M106	S1.9	SABbc	7.2[c]	9.10	12 18 57.5	+47 18 14.3
NGC 4388		S1.9	Sb: spin	16.7	11.76	12 25 46.7	+12 39 40.9
NGC 4395		S1.5*	Sm:	4.1[d]	10.64	12 25 48.9	+33 32 47.8
NGC 4472	M49	S2::	E2	16.7	9.37	12 29 46.8	+07 59 59.9
NGC 4477		S2	SB0?	16.8	11.38	12 30 02.2	+13 38 11.3
NGC 4501	M88	S2	Sb	16.8	10.36	12 31 59.3	+14 25 13.4
NGC 4565		S1.9	Sb? spin	9.7[c]	10.42	12 36 21.1	+25 59 13.5
NGC 4579	M58	S1.5/L1.5*	SABb	16.8	10.48	12 37 43.4	+11 49 04.9
NGC 4639		S1.5*	SABbc	16.8	12.24	12 42 52.5	+13 15 24.1
NGC 4698		S2	Sab	16.8	11.46	12 48 22.9	+08 29 14.8
NGC 4725		S2:	SABab pec	13.0[c]	10.11	12 50 26.7	+25 30 02.3
NGC 5033		S1.5	Sc	18.7	10.75	13 13 27.5	+36 35 37.8
NGC 5194	M51	S2	Sbc pec	8.4	8.96	13 29 52.4	+47 11 40.8
NGC 5273		S1.5	S0	16.5[c]	12.44	13 42 08.3	+35 39 15.2

Notes: Col. (1); galaxy name; Col. (2): other name; Col. (3): optical classification as given by HFS97a: "S" represents Seyfert, "L" represents LINER, and "T" represents objects with LINER plus H II-region spectra. "2" implies that no broad Hα is detected; "1.9" implies that broad Hα is present, but not broad Hβ; "1.5" implies that both broad Hα and broad Hβ are detected, with substantial contributions from both the BLR and NLR (Osterbrock 1981). Objects with a changed classification with respect to the original given by HFS97a (see also Ho et al. 1997b and HU01) are denoted by "*" after their name; Col. (4): Hubble type as listed in HFS97a; Col. (5): distance from Tully (1988), except when marked with ([a]) Paturel et al. (2002), ([b]) Cecil et al. (2002), ([c]) Tonry et al. (2001), and ([d]) Thim et al. (2004); Col. (6): total apparent B_T magnitude of the galaxy; Cols. (7)–(8): nuclear optical position in epoch J2000 as given by HU01. N.B: Two sources (NGC 3031 and NGC 4579) have classifications which fall near the somewhat arbitrary boundary between a Seyfert and a LINER, depending on the adopted criteria. Because they are on the Seyfert side in HFS97a, they are included here and classified as "S/L". In objects like NGC 676, NGC 2685, NGC 3185, NGC 4472, and NGC 4725, the starlight subtraction process has been particularly difficult, leading to uncertain classifications. Following HFS97b, we marked these sources with a quality rating ":" (uncertain) or "::" (highly uncertain).

ranging between 5 and 50 ks, with typical values around 15 ks. Remaining objects were taken from the *XMM–Newton* Science Archive. All sources were observed with the EPIC CCDs (MOS and pn) as the prime instrument.

Observation dates, exposure times, and filters used during the observations are listed in Table 2. The raw observation data files (ODFs) were reduced and analyzed using the standard Science Analysis System (SAS) software package (version 5.3, released in June 2002; Saxton 2002) with associated latest calibration files. We used *epproc* and *emproc* tasks for the pipeline processing of the ODFs to generate the corresponding event files and remove dead and hot pixels. Time intervals with very high background rates were identified in light curves at energy >10 keV and removed. Only patterns ≤12 for "MOS" and ≤4 for "pn" were considered in the analysis and a standard selection filter of FLAG = 0 was applied.

3. Spatial and timing analysis

Images and light curves were analyzed in the 0.5–2 keV (soft) and 2–10 keV (hard) energy bands, for MOS and pn separately. Despite the short exposures (as low as ∼5 ks; see Table 2), all targets are detected with a minimum of 20 counts per detector in either the soft or the hard energy band. Flux limits reached are on the order of $F_{(0.5-2\ \mathrm{keV})} \approx 10^{-14}$ erg cm^{-2} s^{-1} and $F_{(2-10\ \mathrm{keV})} \approx 10^{-13}$ erg cm^{-2} s^{-1}. These flux limits translate into minimum luminosities detectable of $\sim 10^{38}$ erg s^{-1}

Table 2. Observation summary.

Galaxy name (1)	Start date (UT) (2)	Obs. orbit (3)	Exposure (s) M1/M2/pn (4)	Filter M1/M2/pn (5)
NGC 676	2002-07-14	475	17296/17578/15757	thin/thin/thick
NGC 1058	2002-02-01	393	11749/11798/6574	thin/thin/med
NGC 1068	2000-07-29	117	38351/34735/33521	med/med/med
NGC 2685	2001-10-15	339	6397/6687/4841	thin/thin/thin
NGC 3031	2001-04-22	251	-/-/84400*	-/-/med*
NGC 3079	2001-04-13	246	21434/21776/10922	med/med/thin
NGC 3185	2001-05-07	258	11791/12117/8041	thin/thin/thick
NGC 3227	2000-11-28	178	36514/36517/32579	med/med/med
NGC 3486	2001-05-09	259	4600/4663/5061	thin/thin/med
NGC 3941	2001-05-09	259	6233/6286/5302	thin/thin/med
NGC 4051	2002-11-22	541	47814/48311/41889	med/med/med
NGC 4138	2001-11-26	360	13575/13567/8856	thin/thin/med
NGC 4151	2000-12-21	190	29233/29253/21241	med/med/med
NGC 4168	2001-12-04	364	21886/21916/16009	thin/thin/med
NGC 4258	2000-12-08	183	20224/20246/13535	med/med/med
NGC 4388	2002-07-07	472	8768/8798/3866	med/med/thin
NGC 4395	2002-05-31	562	37096/30453/10873	thin/thin/thin
NGC 4472	2002-06-05	456	15181/15300/11043	thin/thin/thin
NGC 4477	2002-06-08	457	13329/13393/8457	thin/thin/med
NGC 4501	2001-12-04	364	12645/12637/2565	thin/thin/med
NGC 4565	2001-07-01	286	14100/14113/8912	thin/thin/med
NGC 4579	2003-06-12	642	19568/20015/15396	thin/thin/thin
NGC 4639	2001-12-16	370	13672/13683/8863	thin/thin/med
NGC 4698	2001-12-16	370	14321/14427/8961	thin/thin/med
NGC 4725	2002-06-14	460	17062/17076/11941	thin/thin/med
NGC 5033	2001-07-02	286	7372/7232/869	thin/thin/med
NGC 5194	2003-01-15	568	20429/20465/17218	thin/thin/thin
NGC 5273	2002-06-14	460	15414/15474/9263	thin/thin/med

Notes: Col. (1): galaxy name; Col. (2): observation start date; Col. (3): observation orbital period; Col. (4): cleaned exposure of MOS1/MOS2/pn; Col. (5): filters used for MOS1/MOS2/pn; "*" means that MOS1 was not considered because it was operated in fast uncompressed mode, and MOS2 was not considered because it was operated in full-frame mode, so the data could thus be affected by pile-up.

and $\sim 10^{39}$ erg s^{-1} for the nearest and farthest Seyferts, respectively.

We find that 25 out of 27 sources, and in particular all type 1 Seyferts, have a compact dominant nucleus coincident with the optical nuclear position reported in Table 1. The only sources that did not display a dominant nucleus were NGC 1058 and NGC 4472, for which upper limits are calculated.

In agreement with recent *Chandra* studies (e.g., Ho et al. 2001; Terashima & Wilson 2003), a wide variety of morphologies is seen. In many cases a bright point-like nucleus is present; in other cases, the nuclear (arcmin size) regions are characterized by the presence of structures, off-nuclear sources, and/or diffuse emission. An atlas of *XMM–Newton* and *Chandra* images of the all sample is given by Panessa (2004). Adopting the classification scheme proposed by Ho et al. (2001), which separates the morphologies in four classes (according to the predominance of the nuclear emission with respect to the surrounding structures), we find that the most common morphology is that of a single compact nucleus centered on the position of the optical nucleus (~60% of the sources), followed by those having a nucleus comparable in brightness to off-nuclear sources in the galaxy (~25%), and a few percent have their nuclei embedded in diffuse soft emission or no core emission. There is also good agreement between the *XMM–Newton* and *Chandra* classifications, which guarantees that the *XMM–Newton* point-spread function (PSF) is effective enough to exclude contamination from off-nuclear sources.

Analysis of the soft and hard X-ray light curves indicates that most sources do not exhibit significant flux variations, except for the few brightest Seyfert 1 galaxies (i.e., NGC 3227, NGC 4051, NGC 4151, NGC 4395) for which the detailed timing analysis is deferred to specific papers presented in the litterature and cited in the Appendix. However, this is not inconsistent with the expectation that low luminosity sources should exhibit higher variability amplitude (Nandra et al. 1997) because, given the low statistics, flux variations up to a factor of a few cannot be excluded for most sources. We thus ignored here any potential spectral variations and considered only the source *average* X-ray spectra which are the subject of our study. This assumption should, however, be kept in mind.

4. Spectral analysis

Source spectra were extracted from circular regions with radii of 50″ and 25″ for sources brighter and fainter than $F_{(0.5-10\ \mathrm{keV})} \approx 10^{-13}$ erg cm^{-2} s^{-1}, respectively, except where

Table 3. Best-fit parameters for the X-ray spectral analysis.

Galaxy name	$N_{H_{Gal}}$	N_H	Γ_{HX}	Γ_{SX}	kT	EW(Fe K)	χ^2_{red}/ν	F_{SX}	F_{HX}	log $L^{int.}_{SX}$	log $L^{int.}_{HX}$
(1)	(2)	(3)	(4)	(5)	(6)	(7)	(8)	(9)	(10)	(11)	(12)
NGC 676	4.4	≤0.1	1.9 ± 0.3	–	–	–	1.2/12	0.1	0.2	38.9	39.0
NGC 1058‡	6.7	≤0.6	1.3 ± 0.9	–	–	–	0.2/2	<0.1	<0.4	<38.1	<38.6
NGC 1068†*	3.5	≤0.1	1.0 ± 0.1	3.5 ± 0.5	0.7 ± 0.2	1200 ± 500	4.3/1399	111.3	46.2	41.4	41.1
NGC 2685	4.1	≤0.3	0.5 ± 0.2	–	–	–	1.5/8	0.2	2.7	38.8	39.9
NGC 3031*	4.1	≤0.1	1.9 ± 0.1	–	0.6 ± 0.1	40 ± 20	1.2/1651	87.0	120.0	40.2	40.3
NGC 3079†	0.8	0.05 ± 0.03	1.7 ± 0.1	–	0.7 ± 0.1	1480 ± 500	1.1/264	<2.5	3.3	<40.0	40.1
NGC 3185	2.1	≤0.2	2.1 ± 0.1	–	–	–	0.6/5	0.2	0.2	39.0	39.0
NGC 3227	2.2	6.8 ± 0.3	1.5 ± 0.1	$\equiv\Gamma_{HX}$	–	190 ± 40	1.1/1863	4.0	81.4	41.2	41.7
NGC 3486	1.9	≤0.3	0.9 ± 0.2	–	–	–	1.1/6	0.2	1.1	38.0	38.9
NGC 3941	1.9	≤0.1	2.1 ± 0.3	–	–	–	1.8/8	0.4	0.4	38.8	38.9
NGC 4051*	1.3	≤0. 3	1.2 ± 0.1	3 ± 0.5	0.2 ± 0.1	240 ± 40	2.2/2006	47.3	62.7	41.2	41.3
NGC 4138	1.4	8.0 ± 1	1.5 ± 0.1	$\equiv\Gamma_{HX}$	0.3 ± 0.1	83 ± 30	1.0/408	0.6	55.0	40.9	41.3
NGC 4151*	2.0	7.5 ± 1	1.6 ± 0.2	1.8 ± 0.5	–	300 ± 30	1.9/2785	29.7	451.0	42.0	42.5
NGC 4258†	1.2	8.7 ± 0.3	1.7 ± 0.1	1.9 ± 0.1	0.5 ± 0.1	27 ± 20	1.0/899	<3.4	83.7	<40.7	40.9
NGC 4388	2.6	27 ± 2	1.3 ± 0.2	$\equiv\Gamma_{HX}$	0.3 ± 0.1	450 ± 70	1.0/283	2.2	76.2	41.2	41.8
NGC 4395	1.3	5.3 ± 0.3	1.2 ± 0.1	$\equiv\Gamma_{HX}$	0.2 ± 0.1	100 ± 25	0.97/535	1.0	61.6	39.2	39.8
NGC 4472‡	1.7	0.3 ± 0.1	2.7 ± 0.3	–	0.8 ± 0.2	–	1.8/483	<19.8	<3.8	<40.8	<40.1
NGC 4477	2.6	≤2	1.9 ± 0.3	–	0.4 ± 0.1	–	1.0/106	<2.0	1.2	<40.0	39.6
NGC 4501	2.5	≤0.2	1.5±0.3	–	0.4 ± 0.1	–	1.1/28	0.9	1.1	39.5	39.6
NGC 4565	1.3	0.12 ± 0.04	1.8 ± 0.2	–	–	–	1.2/70	1.1	2.4	39.2	39.4
NGC 4579	2.4	≤0.02	1.7 ± 0.1	–	0.6 ± 0.1	170 ± 50	1.1/1043	25.3	38.5	41.0	41.1
NGC 4639	2.4	≤0.01	1.8 ± 0.1	–	–	–	1.0/176	3.0	4.9	40.0	40.2
NGC 4698	1.9	≤0.4	2.0 ± 0.2	–	–	–	1.2/17	0.3	0.4	39.1	39.2
NGC 4725	0.1	≤5	1.9 ± 0.5	–	0.3 ± 0.1	–	0.84/44	0.7	0.4	39.2	38.9
NGC 5033	0.1	≤0.03	1.7 ± 0.1	–	–	466 ± 215	0.97/335	15.0	28.7	40.8	41.1
NGC 5194	1.6	≤0.03	0.6 ± 0.1	–	0.5 ± 0.1	986 ± 210	1.65/361	7.3	4.8	39.8	39.6
NGC 5273	0.1	0.9 ± 0.1	1.4 ± 0.1	$\equiv\Gamma_{HX}$	0.2 ± 0.1	226 ± 75	1.1/1009	13.2	67.1	41.0	41.4

Notes: SX = 0.5–2 keV, HX = 2–10 keV. Galaxies marked with † and ‡ indicate that the nuclear regions are contaminated (by more than 10%) by off-nuclear point-sources and/or diffuse emission in only the soft band (†) or in both the soft and hard bands (‡). Galaxies marked with "*" indicate sources with very complex spectra for which only a rough parametrization is given here. See Appendix B for more details on individual sources; Col. (1): galaxy name; Col. (2): Galactic absorption along the line of sight, in units of 10^{20} cm^{-2}; Col. (3): measured absorption column density, in units of 10^{22} cm^{-2}; Col. (4): power-law photon index; Col. (5): photon index of the soft power-law component; Col. (6): temperature of the thermal component (kT) in units of keV; Col. (7): equivalent width of the Fe K line, in units of keV; Col. (8): reduced chi-squared and number of degrees of freedom. Columns (9)–(10): observed fluxes in the soft (0.5–2 keV) and hard (2–10 keV) X-ray bands, in units of 10^{-13} erg cm^{-2} s^{-1}; Cols. (11)–(12): Log of the absorption-corrected luminosities in the soft (0.5–2 keV) and hard (2–10 keV) X-ray bands (computed using distances from Table 1).

noted in Appendix B. These extraction regions correspond to energy encircled fractions of ∼90% and ∼80%, respectively. When available, we have looked at *Chandra* images in order to check for possible contamination due to off-nuclear sources or diffuse emission unresolved by *XMM–Newton*. Sources which may have been affected by this type of contamination are marked with "†" (only soft) or "‡" (both soft plus hard) in Table 3, which lists the best-fit spectral parameters. The background was estimated using standard blank-sky files or, when unusually high (as in the case of NGC 5033), locally from source-free circular regions placed in offset positions close to the source.

Spectral channels were binned to a minimum of 20 counts per bin and spectra were fitted using data from the three CCD detectors (MOS1/2 and pn) simultaneously. The pn normalization is fixed to 1, while the MOS1/2 normalizations are left free to vary in the range 0.95–1.05 to account for the remaining calibration uncertainties in their cross-normalizations[3]. Statistical errors are in any case typically much larger than current calibration uncertainties. Data were fitted in the range 0.3–10 keV for MOS1/2 and 0.5–10 keV for the pn.

Spectral analysis was performed to first identify the underlying continuum when possible, and then additional components and features were included to best reproduce the data. Hence, each spectrum was initially fitted with a single model consisting of a power law plus absorption fixed at the Galactic value as quoted in Col. (2) of Table 3, plus intrinsic absorption as quoted in Col. (3).

In many cases this simple parametrization is not sufficient to model the whole 0.3–10 keV spectrum. Residuals

[3] See `http://xmm.vilspa.esa.es/external/xmm_sw_cal/calib/index.shtml`

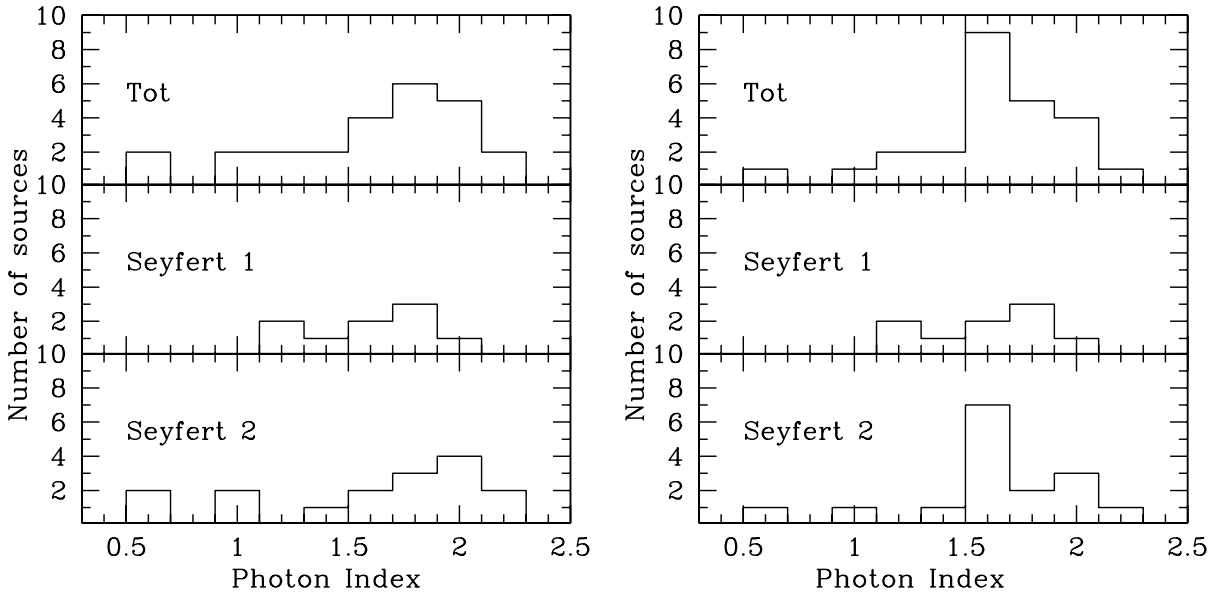

Fig. 1. Distribution of the photon index before (*left*) and after (*right*) correction for Compton-thick candidates (after Table 4) for which a value of $\Gamma = 1.62$ is assumed (see text for details).

often show, for example, a soft excess on top of the (absorbed or non-absorbed) power law. The soft-excess component is clearly more complex than a single power law, often exhibiting emission or absorption structures, or both. The soft excess is fitted here using a simple, and approximate, description/parameterization in terms of a scattered power-law component (with index given in Col. (5)) plus a thermal plasma model (with temperature kT given in Col. (6), and metallicity fixed to the solar value). The possible presence of a narrow emission line centered at 6.4 keV originating from neutral iron has also been checked, and modeled with a single Gaussian line (with equivalent width, *EW*, given in Col. (7)). Best-fit spectral parameters are reported in Table 3. Errors given in the table are calculated at 90% confidence for two interesting parameters ($\Delta\chi^2 = 4.61$), and we applied a single-digit approximation.

It is stressed that some source spectra, in particular those with high-quality statistics, do clearly require more complex modeling of the continuum and additional narrow absorption and/or emission features than used above in our simplified procedure. For example, NGC 3227, NGC 4051, NGC 4151, NGC 4395, and NGC 5273 show additional continuum curvatures in the residuals which indicate either multiple or ionized absorption. The same is true for NGC 1068 and NGC 4051 for which a reflection continuum in the data is likely to be significant. Other sources such as NGC 1068, NGC 3031, NGC 3079, NGC 4051, NGC 4151, and NGC 5273 also show evidence for additional absorption and/or emission structures at soft and/or hard energies. Given the purpose of this work (to obtain a proper, uniform, average description of the spectra in terms of absorption, photon-index continuum, flux, and Fe K line intensity), we do not attempt to fit all these extra components in a systematic way. Rather, we address these issues case-by-case in Appendix B, where references from the literature are also quoted, and we take these caveats into account when interpreting the overall spectral results.

5. X-ray properties

5.1. Observed values of Γ, $N_{\rm H}$, and $L_{2-10\ \rm keV}$

Figure 1 (upper panel) reports the distribution of best-fit photon indices. These vary from object to object over the range $0.5 < \Gamma < 2.3$ (the value $\Gamma = 2.7$ for NGC 4472 is excluded here because it is due to diffuse emission from the galaxy; see Appendix B). The weighted mean for the total sample is $\Gamma \approx 1.60 \pm 0.04$, with a dispersion $\sigma \approx 0.44$. The distribution for type 1 objects (middle panel of Fig. 1) has a mean value of 1.56 ± 0.04 and a dispersion $\sigma \approx 0.24$. The rather flat ($\Gamma \lesssim 1.5$) spectrum of 4 (out of 9) type 1 objects can be ascribed to either the presence of a warm absorber, a complex absorber, and/or a reflection component, all of which produce a flattening of the continuum. The distribution of Γ for type 2 objects (lower panel of Fig. 1) is somewhat broader. The weighted mean for this class is 1.61 ± 0.06 with a dispersion of ~0.5. A Kolmogorov-Smirnov (KS) test gives a probability of ~0.43, consistent with the same parent population.

Figure 2 (left panel) shows the observed column density distribution obtained for the total sample (top panel), type 1 (middle panel), and type 2 (bottom panel) Seyfert galaxies. Arrows indicate upper limits. The observed total distribution varies over the range of Galactic absorptions ($N_{\rm H} \approx 10^{20}$ cm^{-2}) to high column densities ($N_{\rm H} \lesssim 10^{24}$ cm^{-2}), with most of the measurements being upper-limits of $N_{\rm H} \approx 10^{21-22}$ cm^{-2}. Type 1 objects are known to be less absorbed than type 2 s, but three of them show a column density higher than 10^{22} cm^{-2}. The nature of the absorbing material in these objects is likely associated with highly ionized gas (NGC 3516, Netzer et al. 2002) and/or to dense and variable absorbing columns (NGC 3227, Lamer et al. 2003; NGC 4151, Puccetti et al. 2003).

Past hard X-ray surveys of Seyfert 2 galaxies have revealed that the column density distribution of this class is significantly

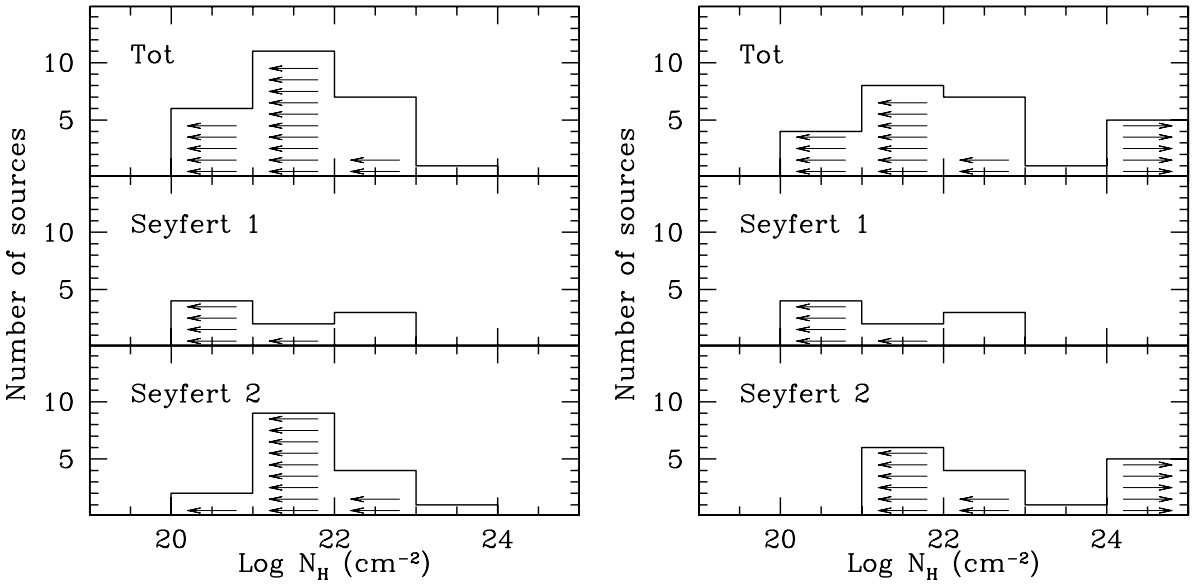

Fig. 2. Distribution of the absorption column densities before (*left*) and after (*right*) correction for Compton-thick candidates (after Table 4). Upper and lower limits are indicated with arrows.

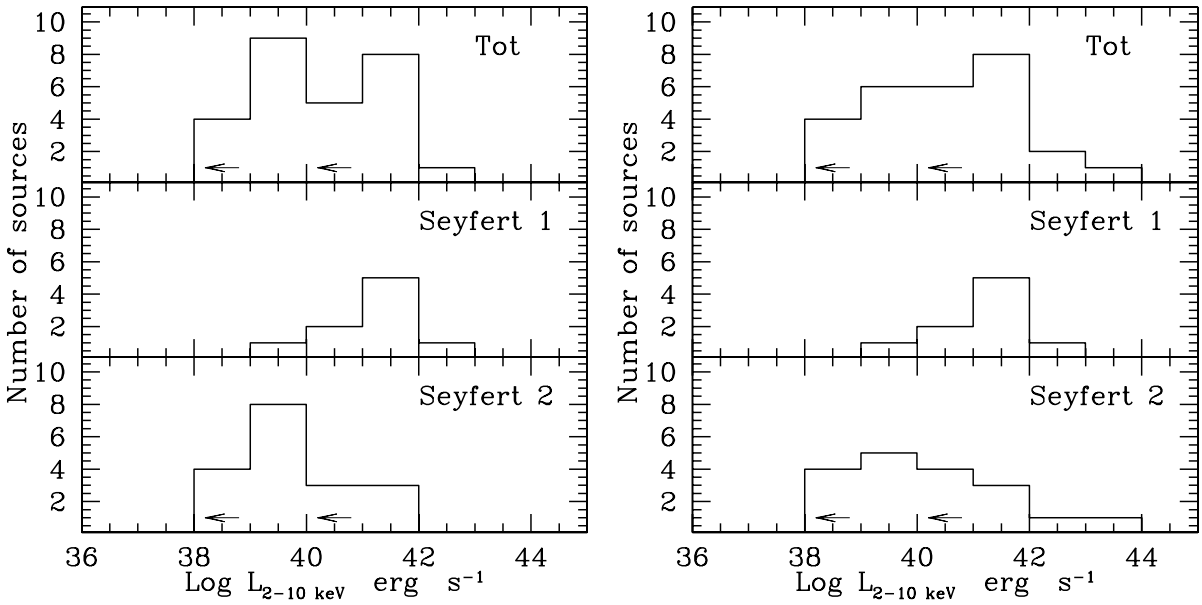

Fig. 3. Distribution of the 2–10 keV luminosities before (*left*) and after (*right*) correction for Compton-thick candidates (after Table 4). Upper limits have been indicated with arrows.

shifted toward large columns; most (~75%) of type 2 Seyferts are heavily obscured, with $N_H > 10^{23}$ cm^{-2} (Risaliti et al. 1999). The distribution observed here and shown in the lower (left side) panel of Fig. 2 apparently deviates from past results, containing mostly mildly absorbed objects. However, this distribution does not take into account the possible presence of heavily absorbed sources, not recognised as such because of the absence of a low energy cut-off.

Histograms of the observed hard X-ray luminosities are shown in Fig. 3 (left side). A wide range of luminosities is covered, from objects with $L_{2-10keV} \approx 10^{38}$ erg s^{-1}, comparable to those of bright binary systems or ultraluminous X-ray sources (ULXs), to those with luminosities $L_{2-10\ keV} \approx 10^{43}$ erg s^{-1}, typical of bright Seyferts. The upper limits on the hard luminosity for the two type 2 Seyferts (NGC 1058 and NGC 4472) are indicated with arrows. It has been shown in previous soft and hard X-ray surveys that Seyfert 2 galaxies are generally weaker than their type 1 counterparts. Our measurements confirm, at first glance, this evidence. A KS test to compare the two distributions yields a probability of 0.009 that they are drawn from the same parent population. The mean hard X-ray luminosity of type 1 objects is $L_{2-10\ keV} \approx 10^{41}$ erg s^{-1} ($\sigma \approx$ 0.8), while for type 2 objects it is $L_{2-10\ keV} \approx 10^{39.8}$ erg s^{-1} ($\sigma \approx 0.9$).

A Gaussian iron K emission line has been detected in 8 out of 9 type 1s and in 6 out of 18 type 2s. Their mean equivalent widths are ≈215 ± 80 eV and ≈700 ± 220 eV, respectively, which are consistent with previous works (Nandra et al. 1997;

Turner et al. 1997) when the large errors and dispersions are taken into account. The larger rate of detected lines in type 1s with respect to type 2s is at first surprising but is consistent with the fact that type 1s are typically brigther in the sample. As mentioned in Sect. 4, the present estimates are to be taken as only rough parameterizations because they do not take into account in detail of the multiple lines often present (i.e. in NGC 1068, NGC 3031, NGC 4579), nor the possibility of line broadening (NGC 3031, NGC 4051, NGC 4151, NGC 4395) or variability.

5.2. Identification of heavily absorbed sources

Several of the above differencies in terms of Γ, $N_{\rm H}$ and $L_{2-10\ {\rm keV}}$, could well be due, in part or totally, to our inability to directly measure heavily absorbed sources. In the hard band, the effective area of the pn peaks at energies around 5–6 keV and has an exponential roll-over at higher energies. This implies that we are only weakly sensitive to measurements of absorption columns of $N_{\rm H} \gtrsim 10^{23}$ cm^{-2}. In particular, in Compton-thick sources with $N_{\rm H} > 10^{24}$ cm^{-2}, the transmitted component is completely suppressed below 10 keV and the spectrum observed in the 2–10 keV band is dominated by flattened reprocessed components from a cold and/or warm scatterer (Matt et al. 2000). The galaxy may, thus, be erroneously classified as a source with a flat spectral shape, low absorption and, thus, low luminosity while actually being intrinsically steep, heavily obscured, and luminous (see, for example, the prototypical case of the Seyfert 2 galaxy NGC 1068; Matt et al. 1997; Iwasawa et al. 1997). To take these factors into account, we apply three independent tools to unveil the presence of heavy obscuration: (i) X-ray spectral diagnostics such as flat slope and large Fe Kα *EW*; (ii) flux diagnostic diagrams; and (iii) the $N_{\rm H}$ vs. $F_{2-10\ {\rm keV}}/F_{[{\rm O\ III}]}$ diagram.

In three type 2 objects (NGC 1068, NGC 3079, and NGC 5194), the *EW* of the detected iron K line is higher than ∼1 keV. Such a high value of the *EW* is expected in highly obscured objects since it is measured against a much-depressed continuum ($N_{\rm H} \approx 10^{23}$–$10^{24}$ cm^{-2}; Leahy & Creighton 1993) or against a pure reflection component ($N_{\rm H} > 10^{24-25}$ cm^{-2}; Makishima 1986; Bassani et al. 1999).

In 2 Seyfert 2 galaxies (NGC 2685 and NGC 3486), the photon index is rather flat ($\lesssim$1) and may also be indicative of Compton-thick sources. However, the lack of any strong line makes this criterion alone not sufficient to classify the sources as Compton-thick candidates. In total, the spectral analysis is able to directly assess three candidate Compton-thick sources, namely NGC 1068, NGC 3079, and NGC 5194. This is consistent with studies which have been able to obtain hard ($E >$ 10 keV) X-ray spectra of these sources with *BeppoSAX* (Matt et al. 1997, Iyomoto et al. 2001; Fukazawa et al. 2001).

Another way of evaluating the true amount of absorption is through flux diagnostic diagrams (e.g., Bassani et al. 1999; Panessa & Bassani 2002; Panessa 2004; Guainazzi et al. 2005). These make use of independent indicators of the intrinsic brightness of the source such as the [O III] λ5007 flux and the infrared emission, to be compared with the hard X-ray flux.

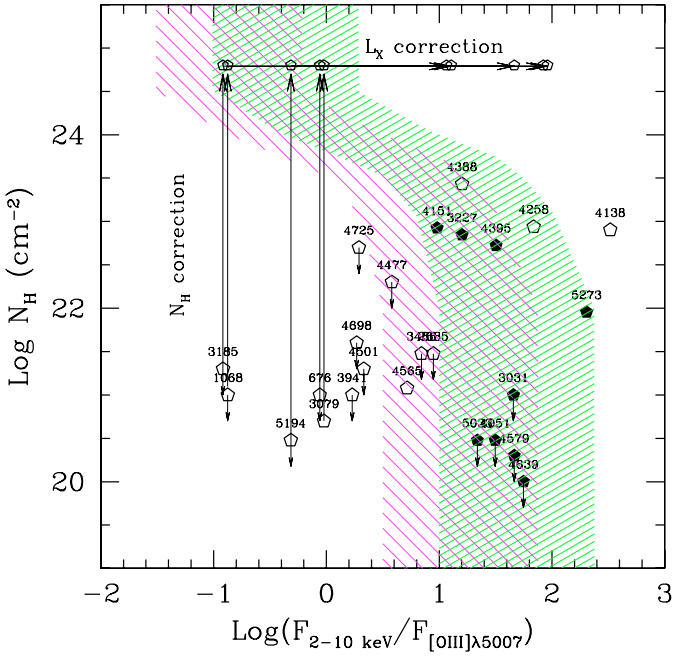

Fig. 4. Diagram of the absorbing column density $N_{\rm H}$ versus the ratio between the observed 2–10 keV flux and the reddening-corrected [O III] flux taken from Panessa (2004). Filled polygons are type 1 Seyferts and open polygons are type 2 Seyferts. The shaded region (lower-left to upper-right diagonals) indicates the expected correlation under the assumption that $L_{2-10\ {\rm keV}}$ is absorbed by the $N_{\rm H}$ reported on the ordinate, starting from the average $F_{\rm HX}/F_{[{\rm O\ III}]}$ ratio observed in type 1 Seyfert galaxies and by assuming a 1% reflected component. Also, the shaded region (upper-left to lower-right diagonals) obtained by Maiolino et al. (1998) is shown.

By studying a large sample of Seyfert 2 galaxies, Bassani et al. (1999) have found that the ratio $F_{2-10\ {\rm keV}}/F_{[{\rm O\ III}]}$ is effective in separating Compton-thin from Compton-thick sources, the latter having ratios lower than ∼1. This is because the [O III] flux is considered to be a good isotropic indicator; it is mostly produced far from the nucleus, in the NLR, by photoionizing photons from the AGN. Applying this criterion to our sample, and using the [O III] measurements reported in HFS97a, we identify 5 Compton-thick sources, i.e. with $F_{2-10\ {\rm keV}}/F_{[{\rm O\ III}]} < 1$: NGC 676, NGC 1068, NGC 3079, NGC 3185, and NGC 5194. Of note is the fact that the three candidates Compton-thick with a strong line are confirmed.

The effectiveness of identifying Compton-thick vs. Compton-thin sources through the ratio $F_{2-10\ {\rm keV}}/F_{[{\rm O\ III}]}$ is also exemplified by the third of our diagnostics: the $N_{\rm H}$ vs. $F_{2-10\ {\rm keV}}/F_{[{\rm O\ III}]}$ diagram shown in Fig. 4. Assuming, as mentioned above, that the [O III] luminosity is an isotropic indicator of the intrinsic luminosity, one expects that the ratio of $F_{2-10\ {\rm keV}}/F_{[{\rm O\ III}]}$ decreases as $N_{\rm H}$ increases, following a path as indicated by the dashed region in Fig. 4. The relation was obtained assuming that the observed $F_{2-10\ {\rm keV}}$ changes according to the $N_{\rm H}$ value given on the ordinate, and starting from the average $F_{2-10\ {\rm keV}}/F_{[{\rm O\ III}]}$ ratio observed in type 1 Seyferts and assuming a 1% scattered component. The width of the shaded area (from lower left to upper right) was drawn considering the lower and higher $F_{2-10\ {\rm keV}}/F_{[{\rm O\ III}]}$ ratios obtained for the

Table 4. Compton-thick/thin Seyfert 2 candidates.

Name	$\Gamma_{2-10\ \mathrm{keV}}$	$EW_{\mathrm{Fe\ K}}$	Flux diag.	Thick?
(1)	(2)	(3)	(4)	(5)
NGC 676			Thick	√
NGC 1058			Thick/SB	?
NGC 1068	Thick	Thick	Thick	√
NGC 2685	Thick		Thin	?
NGC 3079		Thick	Thick	√
NGC 3185			Thick	√
NGC 3486	Thick		Thick/SB	?
NGC 3941			Thin	×
NGC 4138	Thick	Thin	Thin	×
NGC 4258	Thick	Thin	Thin	×
NGC 4388		Thin	Thin	×
NGC 4472			Thin	?
NGC 4477			Thin	×
NGC 4501	Thin		Thin	×
NGC 4565		Thin	Thin	×
NGC 4698			Thin	×
NGC 4725			Thin	×
NGC 5194		Thick	Thick	√

Notes: "Thick" = Compton-thick candidate, "Thin" = Compton-thin candidate, "SB" = starburst candidate on the basis of spectral diagnostics (Cols. 2 and 3) and flux diagnostics (Col. 4). Final classification (Col. 5): "√" = Compton-thick candidates, "×" = Compton-thin candidate, and "?" = classification uncertain (likely to contain a starburst, but CT nature cannot be excluded).

type 1 objects of the present sample. The shaded region (from upper left to lower right) obtained by Maiolino et al. (1998) is also shown for comparison and is consistent with the present results, though slightly shifted to lower flux ratios.

Compton-thick AGNs should occupy the *observed* low N_{H} and low $F_{2-10\ \mathrm{keV}}/F_{[\mathrm{O\ III}]}$ part of the diagram, but after correction for their *intrinsic* high N_{H}, they should occupy the high N_{H} and low $F_{2-10\ \mathrm{keV}}/F_{[\mathrm{O\ III}]}$ region of the predicted distribution (as indicated by the arrows in Fig. 4). We find that this is indeed the case for the previously identified Compton-thick objects of our sample (NGC 676, NGC 1068, NGC 3079, NGC 3185, and NGC 5194). Other sources (NGC 3941, NGC 4698, and NGC 4501) are located in the same area of the plot, but we found no independent confirmation to classify them as secure Compton-thick candidates. Moreover, they have $F_{2-10\ \mathrm{keV}}/F_{[\mathrm{O\ III}]}$ ratios exceeding 1, in the Compton-thin regime. Interestingly, two of these sources (NGC 4698 and NGC 4501) have been identified in the literature as "anomalous" cases of Seyfert 2 galaxies with no intrinsic absorption (Georgantopoulos & Zezas 2003; Terashima et al. 2002).

By combining the X-ray spectral properties and the diagnostic diagrams using isotropic indicators, we identify Compton-thin and Compton-thick objects as indicated in Table 4. In total, a subsample of 5 Compton-thick candidate objects have been confidently recognized (5 from diagnostic diagrams, 3 of which have direct spectral information as well).

5.3. Γ, N_{H} and $L_{2-10\ \mathrm{keV}}$: after correction for heavily absorbed sources

As a consequence of the above considerations, we correct the above distributions by adopting, for all Compton-thick candidates, a value of $\Gamma = 1.62$, $N_{\mathrm{H}} = 2 \times 10^{24}$ cm^{-2} and increasing $L_{2-10\ \mathrm{keV}}$ by a factor of 100. The first value is taken equal to the average value of Γ in type 2s after removal of the 5 Compton-thick candidates. The second is taken as a lower-limit characteristic value of optically thick matter. The latter value/shift in luminosity is drawn from Fig. 4. This value corresponds, as a rough estimate, to the factor that is necessary to bring the average $F_{2-10\ \mathrm{keV}}/F_{[\mathrm{O\ III}]}$ ratio measured for the 5 Compton thick sources ($\simeq 10^{-0.44}$) equal to that of type 1 sources ($\simeq 10^{1.54}$), as indicated from the arrows in Fig. 4. New histograms are shown in the right-hand panels of Figs. 1–3, where the Compton-thick candidates are marked with right-sided arrows. Although average values do not change significantly before and after this correction, the shapes of the distributions are quite different. The fraction of Compton-thick sources is at least a third of all type 2 Seyferts, and a fifth of all Seyferts. This is similar to what was found by Bassani et al. (1999) using data from the literature and is slightly lower than, but in substantial agreement with the survey by Risaliti et al. (1999) when errors on the percentages are considered. However, the present study adds to the significance of this result because for the first time it is derived using an unbiased (distance-limited) optical sample, applying a uniform optical and X-ray analysis to the data (with data from a single satellite), and excluding any severe contamination from nearby off-nuclear sources.

These findings are, also for the first time, extended down to very low luminosities. Finally, unlike previous studies, no more significant difference between the luminosity distributions of type 1 and type 2 Seyferts are found (Sect. 5.1). The probability of the two classes being drawn from the same parent population is now 0.16. The previous differences in luminosities (Sect. 5.1) are therefore consistent with being ascribed almost entirely to absorption effects.

We have checked that the above results are robust even with slightly different assumptions in correcting for Compton-thick candidates. Assuming a steeper value of $\Gamma = 1.8$ or 1.9, more typical of the *intrinsic* (reflection-corrected) spectrum of unobscured AGNs (Nandra & Pounds 1994), or cancelling out all 5 Compton-thick candidates, similarity between the index distributions of type 1 and type 2s was always recovered. For the luminosity distributions, if we assumed conservatively a correction factor of about 30, i.e. corresponding to the lowest observed value of $F_{2-10\ \mathrm{keV}}/F_{[\mathrm{O\ III}]}$ ratio in type 1s, the KS probability that type 1 and type 2 luminosity distributions are drawn from the same parent population becomes 3×10^{-2} (from a probability of about 10^{-4} when luminosities were not corrected, see Sect. 5.1). This indicates that the above results are, of course, sensitive to the assumptions made to correct for the Compton-thick sources but that even our most conservative choice of correction brings the luminosities of type 2s consistent with that of type 1s.

6. General results and summary

The optical spectroscopic survey of Ho et al. (1995, 1997) has provided a new, comprehensive catalog of 52 Seyfert galaxies, the most complete and least biased available to date. We

have performed an X-ray spectral survey of the 27 nearest ($D \lesssim 22$ Mpc) Seyfert galaxies in that survey using the EPIC CCDs on-board *XMM–Newton*. This paper presents the observational material, along with a compilation of X-ray spectral parameters to be used in subsequent analysis.

We have detected in the hard X-ray band all but two of the observed Seyfert nuclei. The sample extends to significantly lower X-ray luminosities than many previous surveys.

Nuclear X-ray spectra have been obtained forming one of the largest atlases of low-luminosity Seyfert galaxies ever assembled. Simple models have been applied in order to characterize the spectral shape, the presence of absorption in excess of the Galactic value and the presence of an Fe emission line. The distribution of spectral parameters, in particular for type 1 Seyferts, is found to be within the range of values observed in luminous AGNs. At a first glance, the observed column density distribution for type 2 Seyferts appears to be shifted toward low absorbing column densities ($N_{\rm H} < 10^{22}$ cm^{-2}).

Moreover, the observed 2–10 keV luminosity distribution of type 2 Seyfert galaxies appears to be significantly shifted toward low luminosities with respect to type 1 objects. However, the presence of Compton-thick sources in our sample may affect the estimate of these parameters. Therefore, indirect arguments have been used to infer their presence, such as evidence of a flat power-law spectrum in the X-ray band, the presence of a strong Fe Kα line at 6.4 keV, and flux diagnostic diagrams which employ isotropic indicators of the nuclear unobscured emission. Results obtained by combining spectral and flux diagnostic tools indicate that the fraction of heavily obscured objects is large, at least one third of all objects in the sample, in good agreement with previous estimates performed on a flux-limited sample (Risaliti et al. 1999). Interestingly, Seyfert galaxies as a whole possess the entire range of $N_{\rm H}$, from 10^{20} cm^{-2} to 10^{24} cm^{-2}, fairly continuously. This is similar to what was found in the deepest X-ray surveys available to date (Mateos et al. 2005), and it is consistent with local absorption distributions adopted by, e.g., La Franca et al. (2005) to fit the hard X-ray luminosity functions of AGNs.

With the present work we are able to probe much lower luminosities and still find that the fraction of absorbed objects remains significantly high. In light of these findings, the column density and luminosity distributions have been revisited. In particular, it has been shown that the dichotomy observed in the luminosity of type 1 and type 2 Seyferts is mainly due to absorption effects.

We point out a note of caution, however, regarding our ability to identify the Compton-thick cases for the lowest-luminosity sources of the sample. It may be that the statistics are so low that one cannot firmly exclude the possibility that some of them are indeed Compton-thick objects. Correcting for this would of course increase the fraction of Compton-thick sources, and bring the present results to meet with Risaliti et al. (1999) estimates. On the other hand, observational criteria such as those above (flat spectra, 2–10 keV/[O III] ratios, etc.) that are "calibrated" for higher-luminosity objects may not hold for the very low-luminosity AGNs. These may indeed have different spectral energy distributions (e.g., Ho 1999), and hence their X-ray/optical emission-line ratios may not be the same as those of traditional AGNs. Because of these effects, the fraction of Compton-thick sources may vary accordingly, i.e. it could be different in this sample with respect to other previous works because lower-luminosities are probed here. We note, nevertheless, that in these data, we find neither a significant relation between $N_{\rm H}$ and $L_{2-10\ {\rm keV}}$, nor between $N_{\rm H}$ (or $L_{2-10\ {\rm keV}}$) and the source sub-classification.

Another result of this survey is the realization (and statistical quantification) of a number of exceptions to the baseline standard model of Seyfert galaxies. First, at least two objects (M 81 and NGC 4579) show a complex of three distinct emission lines at $E \approx 6.4$, 6.7, and 6.9 keV. Detailed modeling is presented by Dewangan et al. (2004) and Page et al. (2004), but the origin of these lines is not clear. The narrow lines in both objects are like those of LINERs, suggesting possibly different, perhaps transient, emission processes in their nuclear regions (e.g., an advection-dominated accretion flow instead of a thick disk, with or without an outflow or jet; Pellegrini et al. 2000; Blandford & Begelman 1999).

The second exception rests on the fact that at least two, perhaps three, of the Seyfert 2 galaxies show no absorption at all, with stringent upper limits. This is clearly in contrast with a standard unified model, but agrees well with previous findings by Pappa et al. (2001), Panessa & Bassani (2002), Barcons et al. (2003), and Mateos et al. (2005).

The third exception is that our analysis has confirmed that three (out of 9) type 1 galaxies (NGC 4151, NGC 3227, and NGC 4395) show evidence for X-ray absorption, an apparent inconsistency between their optical classification and the X-ray one which has been extensively debated in the literature (Mateos et al. 2005, and refences therein). This is a (30 ± 17)% fraction of absorbed type 1 Seyferts that is consistent with latest estimates based on wide field X-ray surveys (Piconcelli et al. 2003; Perola et al. 2004). All three sources are type 1.5 sources, so there might be an orientation effect where these objects are being viewed from just outside the ionization cone. Other plausible explanations in terms of either effects due to variability in the absorption column density, and/or geometry, and/or ionization state (Malizia et al. 1997; Piro 1999; Risaliti et al. 2002b; Matt et al. 2003), or unusual dust-to-gas ratios have been proposed to explain such differences (Maiolino et al. 2001a,b).

In conclusion, we have given an unbiased estimate of the average intrinsic X-ray properties and column density distribution of Seyfert galaxies at low redshifts. This is crucial to validate unified models of AGNs and for synthesis models of the X-ray background. The results obtained here are in agreement with the predictions of unified models, except for a few particular cases (10% of unabsorbed Seyfert 2s and 30% of absorbed Seyfert 1s, in agreement with previous works by Panessa & Bassani 2002; and Perola et al. 2004) which do not fit easily into the standard picture, but which we are able to quantify. Most significantly, these predictions are positively tested using a complete sample with datasets of unprecedented quality. The first-ever extension to low luminosities also suggests that the same physical processes are governing emission in low-luminosity AGNs as in more luminous sources, although a larger sample is required to verify this conclusion.

A description of the multi-waveband correlations (e.g., X-ray luminosities vs. H_α and radio luminosities, spectral energy distributions, etc.) and their astrophysical implications is deferred to forthcoming papers.

Acknowledgements. This paper is based on observations obtained with *XMM–Newton*, an ESA science mission with instruments and contributions directly funded by ESA Member States and the USA (NASA). The research has made use of data obtained through the High Energy Astrophysics Science Archive Research Center Online Service, provided by the NASA/Goddard Space Flight Center, and of the NASA/IPAC Extragalactic Database (NED), which is operated by the Jet Propulsion Laboratory, California Institute of Technology, under contract with the National Aeronautics and Space Administration. M.C. acknowledges financial support from the contract ASI-CNR/IASF:I/R/042/02. A.V.F. is supported by NSF grant AST–0307894; he is also grateful for a Miller Research Professorship at U.C. Berkeley, during which part of this work was completed.

References

Antonucci, R. R. J. 1993, ARA&A, 31, 473
Awaki, H., Koyama, K., Inoue, H., & Halpern, J. P. 1991, PASJ, 43, 195
Barcons, X., Carrera, F. J., & Ceballos, M. T. 2003, MNRAS, 339, 757
Barth, A. J., Ho, L. C., Filippenko, A. V., Rix, H.-W., & Sargent, W. L. W. 2001, ApJ, 546, 205
Barth, A. J., Reichert, G. A., Filippenko, A. V., Ho, L. C., et al. 1996, AJ, 112, 1829
Bassani, L., Dadina, M., Maiolino, R., et al. 1999, ApJS, 121, 473
Blandford, R. D., & Begelman, M. C. 1999, MNRAS, 303, L1
Caldwell, N., Rose, J. A., & Concannon, K. D. 2003, AJ, 125, 2891
Cecil, G., Bland-Hawthorn, J., & Veilleux, S. 2002, ApJ, 576, 745
Comastri, A., Setti, G., Zamorani, G., & Hasinger, G. 1995, A&A, 296, 1
Dewangan, G. C., Griffiths, R. E., Di Matteo, T., & Schurch, N. J. 2004, ApJ, 607, 788
Eracleous, M., Shields, J. C., Chartas, G., & Moran, E. C. 2002, ApJ, 565, 108
Filippenko, A. V., & Sargent, W. L. W. 1985, ApJS, 57, 503
Filippenko, A. V., & Sargent, W. L. W. 1989, ApJ, 342, L11
Filippenko, A. V., Ho, L. C., & Sargent, W. L. W. 1993, ApJ, 410, L75
Foschini, L., Di Cocco, G., Ho, L. C., et al. 2002, A&A, 392, 817
Fukazawa, Y., Iyomoto, N., Kubota, A., Matsumoto, Y., & Makishima, K. 2001, A&A, 374, 73
Georgantopoulos, I., & Zezas, A. 2003, ApJ, 594, 704
Georgantopoulos, I., Panessa, F., Akylas, A., et al. 2002, A&A, 386, 60
George, I. M., Mushotzky, R., Turner, T. J., et al. 1998, ApJ, 509, 146
Gilli, R., Salvati, M., & Hasinger, G. 2001, A&A, 366, 407
Gondoin, P., Orr, A., Lumb, D., & Siddiqui, H. 2003, A&A, 397, 883
Guainazzi, M., Fabian, A. C., Iwasawa, K., Matt, G., & Fiore, F. 2005, MNRAS, 356, 295
Hasinger, G., Altieri, B., Arnaud, M., et al. 2001, A&A, 365, L45
Heckman, T. M. 1980, A&A, 87, 152
Ho, L. C. 1999, ApJ, 516, 672
Ho, L. C., Filippenko, A. V., & Sargent, W. L. 1995, ApJS, 98, 477
Ho, L. C., Filippenko, A. V., & Sargent, W. L. W. 1997a, ApJS, 112, 315 (HFS97a)
Ho, L. C., Filippenko, A. V., Sargent, W. L. W., & Peng, C. Y. 1997b, ApJS, 112, 391
Ho, L. C., Ptak, A., Terashima, Y., et al. 1999, ApJ, 525, 168
Ho, L. C., & Ulvestad, J. S. 2001, ApJS, 133, 77 (HU01)
Ho, L. C., Feigelson, E. D., Townsley, L. K., et al. 2001, ApJ, 549, L51
Iwasawa, K., Fabian, A. C., & Matt, G. 1997, MNRAS, 289, 443
Iwasawa, K., Fabian, A. C., Almaini, O., et al. 2000, MNRAS, 318, 879
Iwasawa, K., Wilson, A. S., Fabian, A. C., & Young, A. J. 2003, MNRAS, 345, 369
Iwasawa, K., et al. 2005, in preparation
Iyomoto, N., Fukazawa, Y., Nakai, N., & Ishihara, Y. 2001, ApJ, 561, L69
Kinkhabwala, A., Sako, M., Behar, E., et al. 2002, ApJ, 575, 732
La Franca, F., et al. 2005, ApJ, in press [arXiv:astro-ph/0509081]
Lamer, G., Uttley, P., & McHardy, I. M. 2003, MNRAS, 342, L41
Lamer, G., McHardy, I. M., Uttley, P., & Jahoda, K. 2003, MNRAS, 338, 323
Leahy, D. A., & Creighton, J. 1993, MNRAS, 263, 314
Loewenstein, M., Mushotzky, R. F., Angelini, L., Arnaud, K. A., & Quataert, E. 2001, ApJ, 555, L21
Maiolino, R., Salvati, M., Bassani, L., et al. 1998, A&A, 338, 781
Maiolino, R., Marconi, A., Salvati, M., et al. 2001a, A&A, 365, 28
Maiolino, R., Marconi, A., & Olivia, E. 2001b, A&A, 365, 37
Makishima, K. 1986, The Physics of Accretion onto Compact Objects, LNP, 266, 249
Malizia, A., Bassani, L., Stephen, J. B., Malaguti, G., & Palumbo, G. G. C. 1997, ApJS, 113, 311
Mateos, S., Barcons, X., Carrera, F. J., et al. 2005, ArXiv Astrophysics e-prints [arXiv:astro-ph/0506718]
Matt, G., Guainazzi, M., Frontera, F., et al. 1997, A&A, 325, L13
Matt, G., Fabian, A. C., Guainazzi, M., et al. 2000, MNRAS, 318, 173
Matt, G., Guainazzi, M., & Maiolino, R. 2003, MNRAS, 342, 422
Mizuno, T., Ohnishi, T., Kubota, A., Makishima, K., & Tashiro, M. 1999, PASJ, 51, 663
Moran, E. C., Eracleous, M., Leighly, K. M., et al. 2005, AJ, 129, 2108
Nandra, K., & Pounds, K. A. 1994, MNRAS, 268, 405
Nandra, K., George, I. M., Mushotzky, R. F., Turner, T. J., & Yaqoob, T. 1997, ApJ, 476, 70
Netzer, H., Chelouche, D., George, I. M., et al. 2002, ApJ, 571, 256
Ogle, P. M., Marshall, H. L., Lee, J. C., & Canizares, C. R. 2000, ApJ, 545, L81O
Osterbrock, D. E. 1981, ApJ, 249, 462
Page, M. J., Soria, R., Zane, S., Wu, K., & Starling, R. L. C. 2004, A&A, 422, 77
Panessa, F., & Bassani, L. 2002, A&A, 394, 435
Panessa, F. 2004, Ph.D. Thesis, University of Bologna, http://venus.ifca.unican.es/panessa/
Pappa, A., Georgantopoulos, I., Stewart, G. C., & Zezas, A. L. 2001, MNRAS, 326, 995
Paturel, G., Teerikorpi, P., Theureau, G., et al. 2002, A&A, 389, 19
Pellegrini, S., Cappi, M., Bassani, L., et al. 2000, A&A, 353, 447
Perola, G. C., Puccetti, S., Fiore, F., et al. 2004, A&A, 421, 491
Piconcelli, E., Cappi, M., Bassani, L., Di Cocco, G., & Dadina, M. 2003, A&A, 412, 689
Pietsch, W., & Read, A. M. 2002, A&A, 384, 793
Piro, L. 1999, Astron. Nachr., 320, 236
Pounds, K. A., Reeves, J. N., King, A. R., & Page, K. L. 2004, MNRAS, 350, 10
Puccetti, S., Risaliti, G., Fiore, F., et al. 2003, Proc. of the BeppoSAX Symposium: The Restless High-Energy Universe, ed. E. P. J. van den Heuvel, J. J. M. in't Zand, & R. A. M. J. Wijers, in press [arXiv:astro-ph/0311446]
Risaliti, G. 2002, A&A, 386, 379
Risaliti, G., Elvis, M., & Gilli, R. 2002a, ApJ, 566, L67

Risaliti, G., Elvis, M., & Nicastro, F. 2002b, ApJ, 571, 234
Risaliti, G., Maiolino, R., & Salvati, M. 1999, ApJ, 522, 157
Sandage, A., Tammann, G. A., & Yahil, A. 1979, ApJ, 232, 352
Schmitt, H. R., & Kinney, A. L. 1996, ApJ, 463, 498
Schurch, N. J., Warwick, R. S., Griffiths, R. E., & Sembay, S. 2003, MNRAS, 345, 423
Setti, G., & Woltjer, L. 1989, A&A, 224, L21
Shih, D. C., Iwasawa, K., & Fabian, A. C. 2003, MNRAS, 341, 973
Smith, D. A., & Done, C. 1996, MNRAS, 280, 355
Soldatenkov, D. A., Vikhlinin, A. A., & Pavlinsky, M. N. 2003, Astron. Lett., 29, 298
Terashima, Y., Kunieda, H., & Misaki, K. 1999, PASJ, 51, 277
Terashima, Y., Iyomoto, N., Ho, L. C., & Ptak, A. F. 2002, ApJS, 139, 1
Terashima, Y., & Wilson, A. S. 2001, ApJ, 560, 139
Terashima, Y., & Wilson, A. S. 2003, ApJ, 583, 145
Thim, F., Hoessel, J. G., Saha, A., et al. 2004, AJ, 127, 2322
Tonry, J. L., Dressler, A., Blakeslee, J. P., et al. 2001, ApJ, 546, 681
Tully, R. B. 1988, Nearby Galaxies Catalog (Cambridge: Cambridge University Press)
Turner, T. J., George, I. M., Nandra, K., & Mushotzky, R. F. 1997, ApJS, 113, 23
Turner, T. J., George, I. M., Nandra, K., & Mushotzky, R. F. 1998, ApJ, 493, 91
Uttley, P., Fruscione, A., McHardy, I., & Lamer, G. 2003, ApJ, 595, 656
Vaughan, S., Iwasawa, K., Fabian, A. C., & Hayashida, K. 2005, MNRAS, 356, 524
Wu, H., Xue, S. J., Xia, X. Y., Deng, Z. G., & Mao, S. 2002, ApJ, 576, 738
Yang, Y., Wilson, A. S., & Ferruit, P. 2001, ApJ, 563, 124
Young, A. J., & Wilson, A. S. 2004, ApJ, 601, 133
Young, A. J., Wilson, A. S., & Shopbell, P. L. 2001, ApJ, 556, 6

Online Material

Appendix A: Atlas of X-ray spectra

Spectra in order of increasing NGC number are shown. For each object, the upper panel shows the unfolded spectrum and the baseline parameterization, together with the contributions to the model of the various additive components. Residuals are shown in the lower panel in units of σ. Spectral analysis was performed following general "recipes" described in Sect. 4, and as described in the notes on individual sources given in Appendix B.

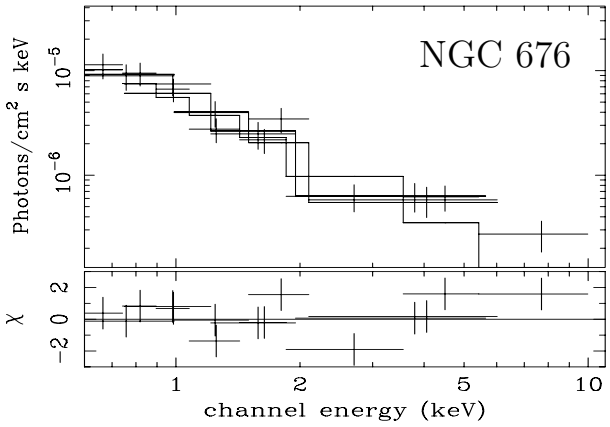
NGC 676
Photons/cm^2 s keV
χ
channel energy (keV)

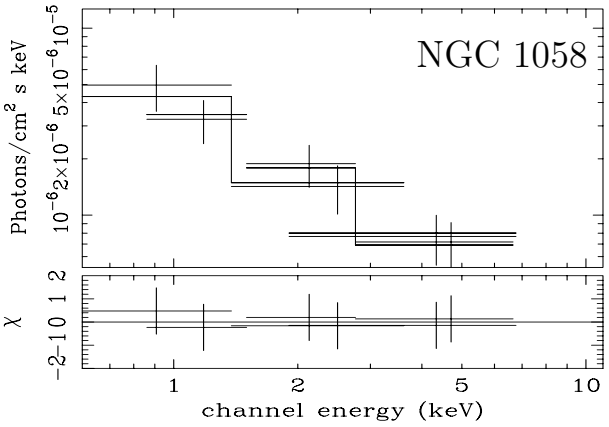
NGC 1058
Photons/cm^2 s keV
χ
channel energy (keV)

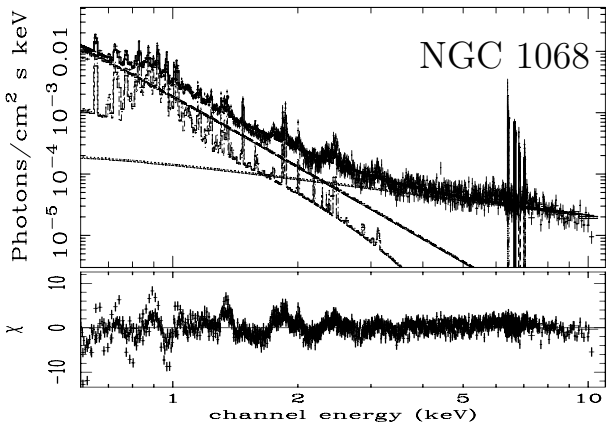
NGC 1068
Photons/cm^2 s keV
χ
channel energy (keV)

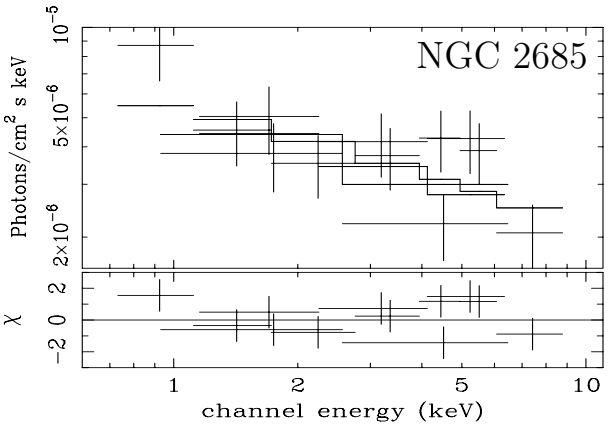
NGC 2685
Photons/cm^2 s keV
χ
channel energy (keV)

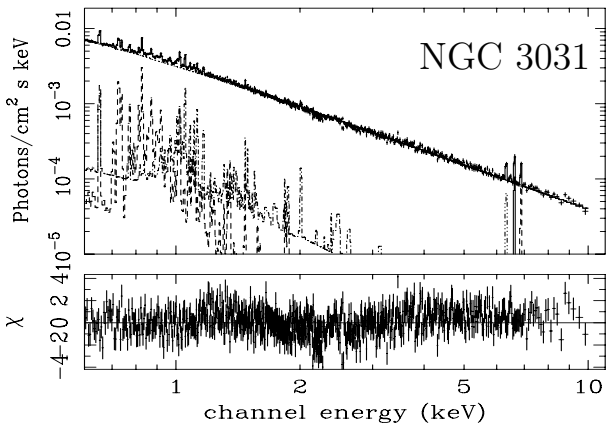
NGC 3031
Photons/cm^2 s keV
χ
channel energy (keV)

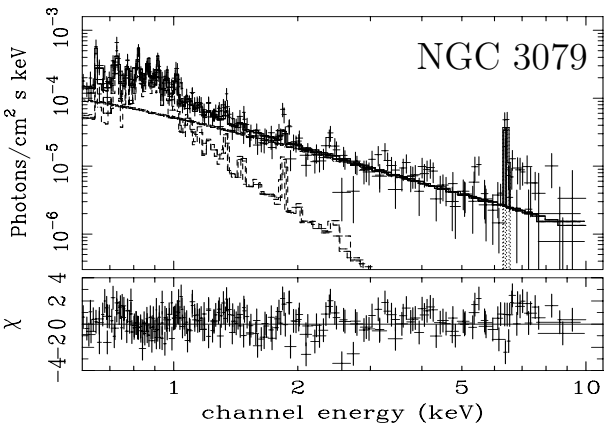
NGC 3079
Photons/cm^2 s keV
χ
channel energy (keV)

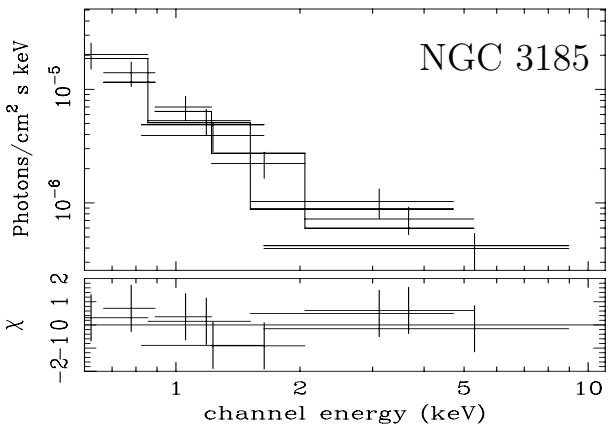
NGC 3185
Photons/cm^2 s keV
χ
channel energy (keV)

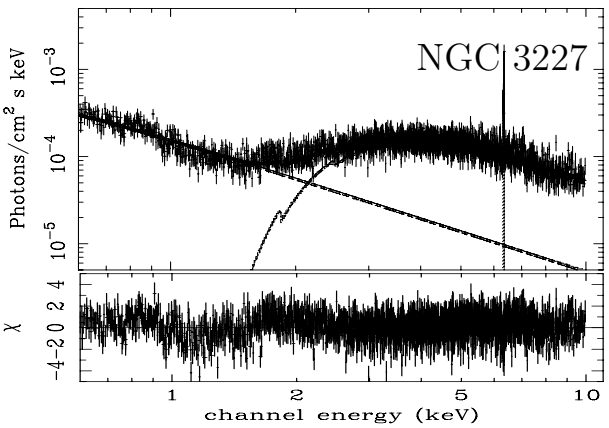
NGC 3227
Photons/cm^2 s keV
χ
channel energy (keV)

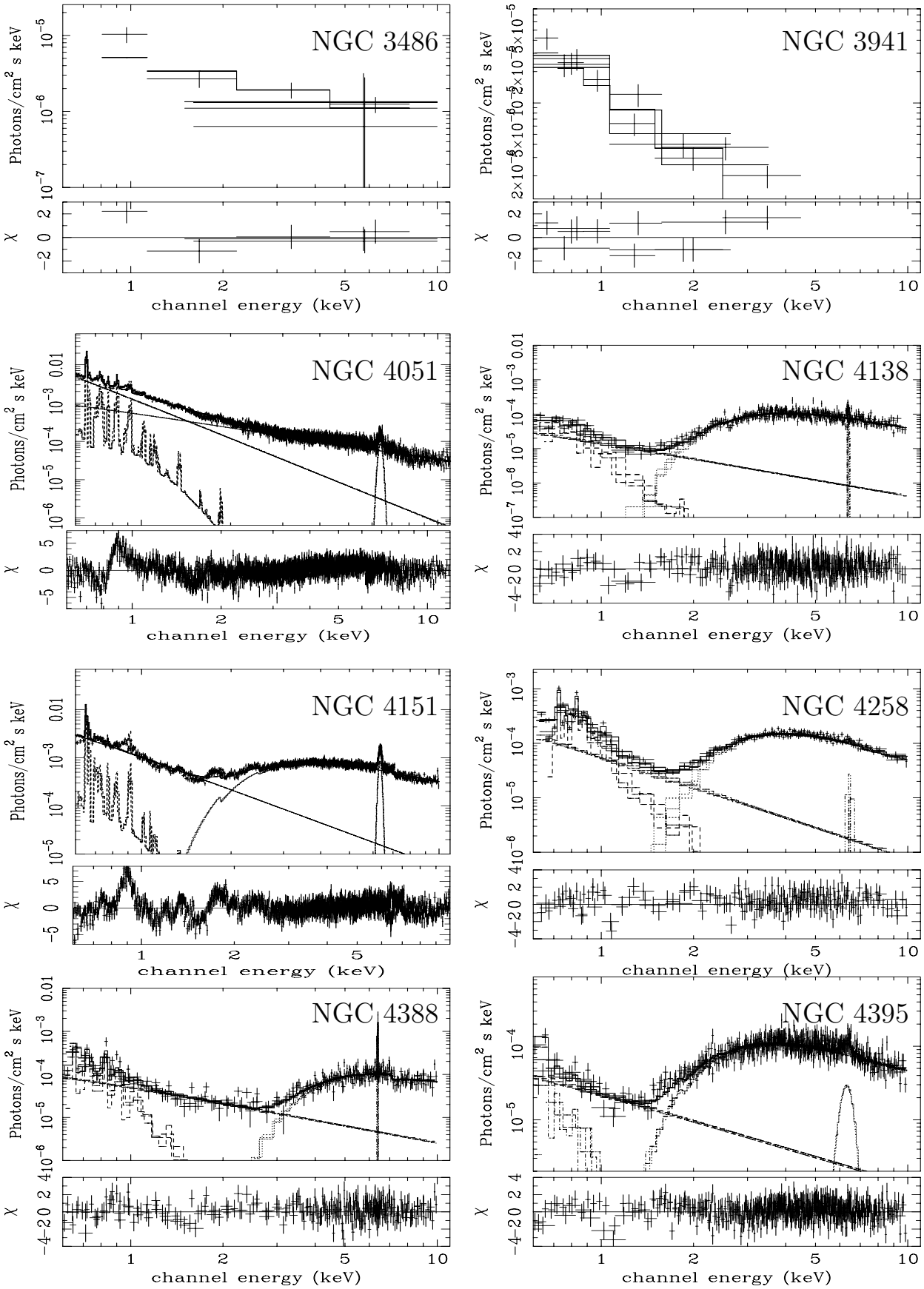
NGC 3486
NGC 3941
NGC 4051
NGC 4138
NGC 4151
NGC 4258
NGC 4388
NGC 4395
Photons/cm^2 s keV
χ
channel energy (keV)

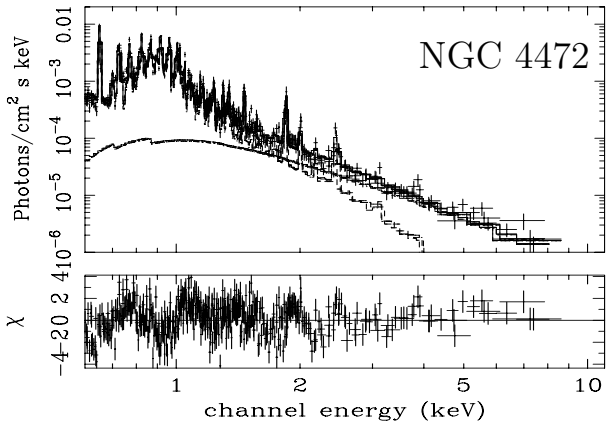
NGC 4472
Photons/cm^2 s keV
χ
channel energy (keV)

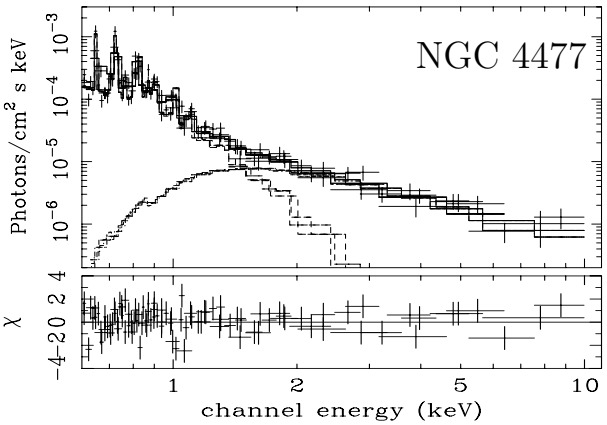
NGC 4477
Photons/cm^2 s keV
χ
channel energy (keV)

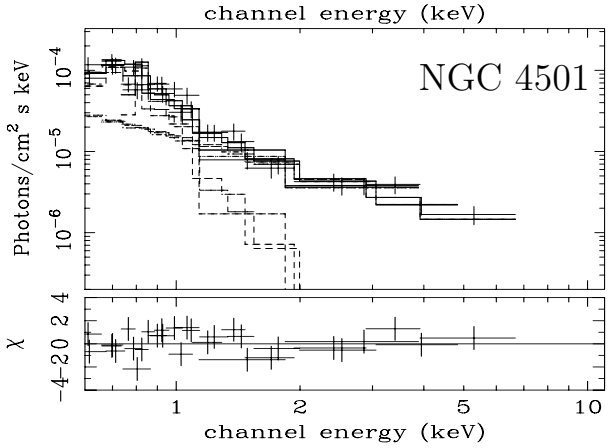
NGC 4501
Photons/cm^2 s keV
χ
channel energy (keV)

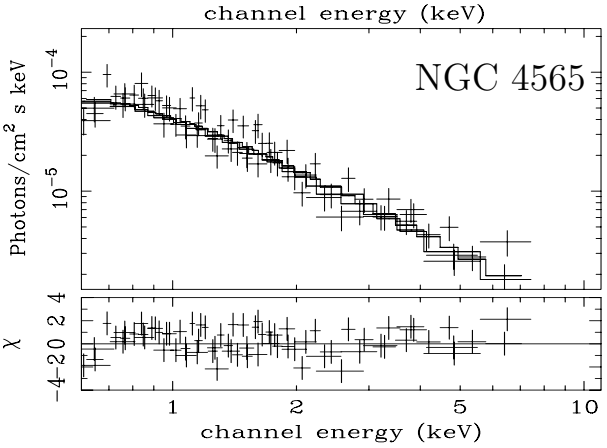
NGC 4565
Photons/cm^2 s keV
χ
channel energy (keV)

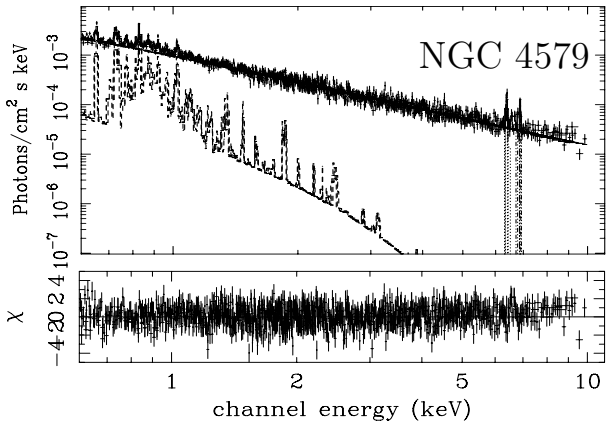
NGC 4579
Photons/cm^2 s keV
χ
channel energy (keV)

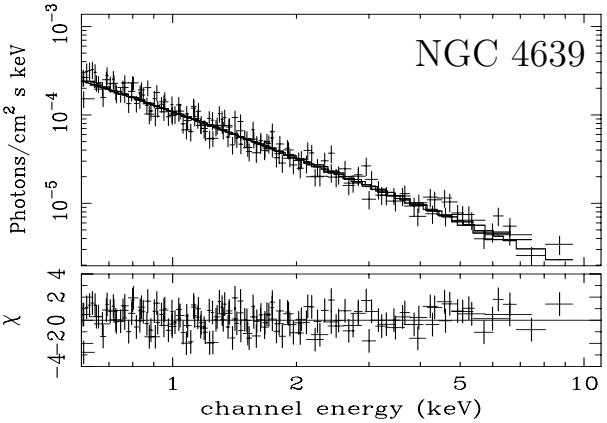
NGC 4639
Photons/cm^2 s keV
χ
channel energy (keV)

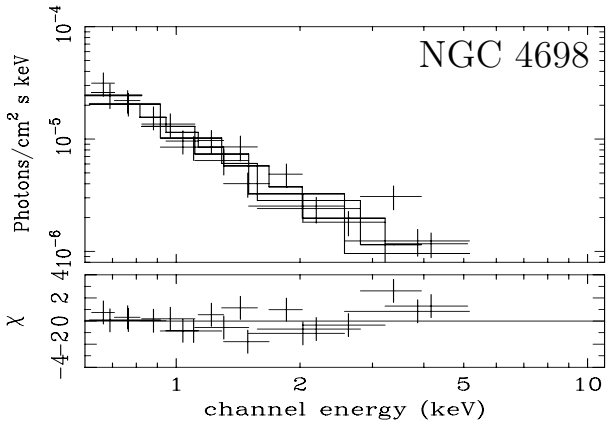
NGC 4698
Photons/cm^2 s keV
χ
channel energy (keV)

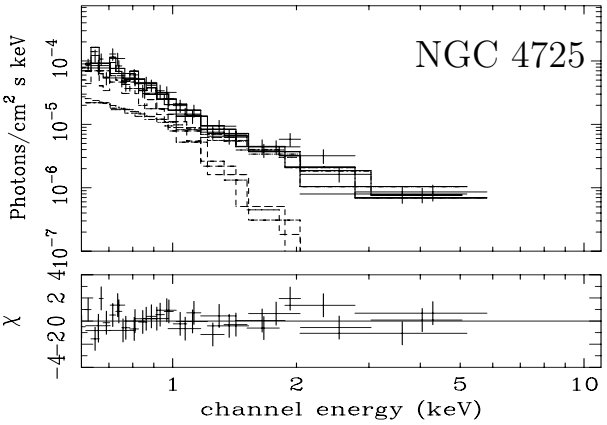
NGC 4725
Photons/cm^2 s keV
χ
channel energy (keV)

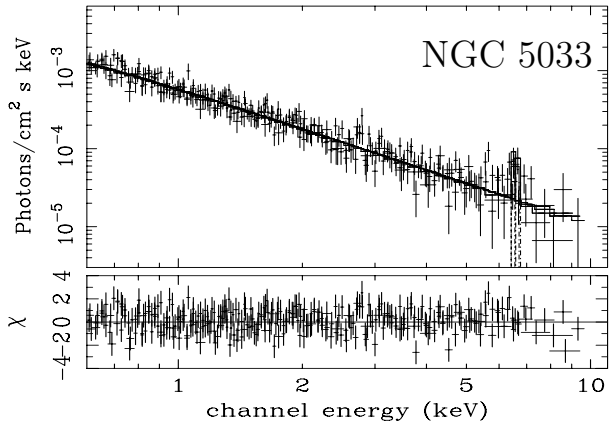
NGC 5033
Photons/cm^2 s keV
χ
channel energy (keV)

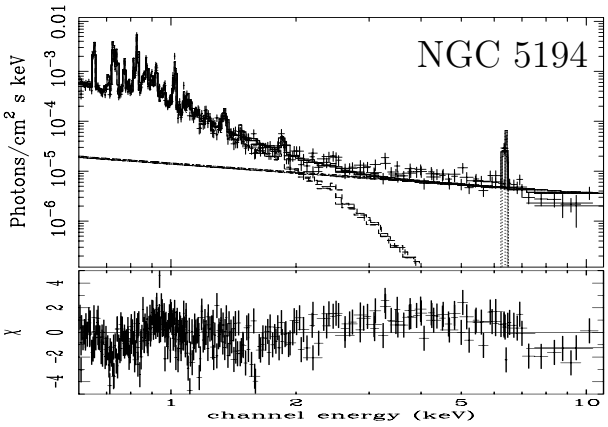
NGC 5194
Photons/cm^2 s keV
χ
channel energy (keV)

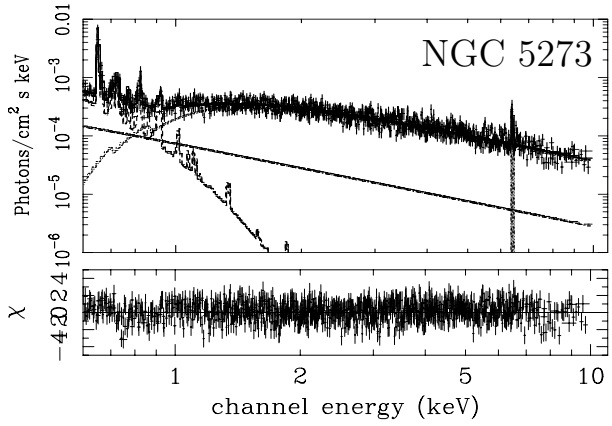
NGC 5273
Photons/cm^2 s keV
χ
channel energy (keV)

Appendix B: Notes on individual objects

In this section we give notes on individual galaxies. In particular, we include a description of (i) the nuclear X-ray morphologies, (ii) the *XMM–Newton* spectral results, and (iii) results from the literature. Spectral best-fit results are discussed only for spectra with more than 100 counts. Bright objects have been observed several times with different X-ray telescopes, but here only the most pertinent literature references are reported. In some cases, *Chandra* images are also used for comparison with the *XMM–Newton* ones and for their superior spatial resolution. An atlas of both *Chandra* and *XMM–Newton* images is given in Panessa (2004).

NGC 676 (S2:): this is the first X-ray detection of NGC 676. The *XMM–Newton* image shows the presence of emission associated with the nuclear optical position and unresolved surrounding emission which might be associated with the nearby off-nuclear sources. The spectrum has poor statistics, but it is described by a power law ($\Gamma = 1.9 \pm 0.1$) with no absorption in excess of the Galactic value. This source has not been detected at radio wavelengths (HU01).

NGC 1058 (S2): there is no strong nuclear core in this object, in agreement with the absence of a radio core detection (HU01). Comparison of the *XMM–Newton* image with the *Chandra* one shows that the 0.5–10 keV flux obtained from the *XMM–Newton* data likely suffers from contamination from an off-nuclear source and thus must be considered as an upper limit.

NGC 1068 (S1.9): *XMM–Newton* images of this source reveal complex nuclear structure: a compact hard nucleus, coincident with the radio core position, embedded in diffuse soft emission. The X-ray spectrum has been thoroughly studied; in particular, the use of the *BeppoSAX*/PDS instrument has confirmed that this is a Compton-thick source (Matt et al. 1997, and references therein). The *XMM–Newton* observation of this source was published by Kinkhabwala et al. (2002), who focused their analysis on the RGS study, and by Matt et al. (2004), who focused their analysis on the $E > 4$ keV data. Here we give only a very rough, approximate description of the 0.5–10 keV spectrum in terms of a soft thermal component, plus a scattered power-law component and a flat power law for the hard X-ray continuum, plus a strong ($EW \approx$ 1–2 keV) Fe complex between 6 and 7 keV (which includes the Fe Kα line at 6.4 keV, plus recombination/resonant emission lines from He-like (6.7 keV) and H-like (6.96 keV) iron, consistent with Matt et al. 2004). Both the flat hard X-ray continuum and the strong Fe line are clear spectral signatures of the Compton-thick nature of this active nucleus.

NGC 2685 (S2/T2:): only weak nuclear emission is revealed in the *XMM–Newton* image, with some faint extended emission associated with the galaxy. The spectrum has poor statistics, yielding a flat power law with low absorption and large uncertainties. The core has not been detected in the radio (HU01).

NGC 3031 (S1.5/L1.5): this is an X-ray bright galactic nucleus extensively studied by most X-ray satellites (Pellegrini et al. 2000; Terashima et al. 2002). A single power law with Galactic absorption plus soft thermal emission gives a good parameterization of the *XMM–Newton* data. Further absorption and/or emission structures are found in the soft energy band, indicating the presence of a complex photoionized and/or thermal plasma. Three Fe lines at different energies (~6.4, 6.7, and 6.9 keV) are detected with equivalent widths on the order of 40–50 eV each. Detailed analysis and interpretation of the complex lines in the *XMM–Newton* dataset are given in two different studies by Dewangan et al. (2004) and Page et al. (2004). A bright and variable radio core is detected (HU01).

NGC 3079 (S2): the *XMM–Newton* images of this source show a complex and unresolved structure which extends for ~30″ around the nuclear position. The hard spectrum is described by a power law ($\Gamma \approx 1.7 \pm 0.1$) modified by little absorption and a strong Fe K line with an EW of almost 2 keV. The 10″-radius region around the nucleus is resolved in the *Chandra* image: the strong nuclear source is embedded in a bubble of diffuse emission. However, the diffuse emission contributes less than 10% of the nuclear emission at $E \gtrsim 2$ keV. A *Chandra* and *HST* study of the superbubble by Cecil et al. (2002) shows that the optical and X-ray emissions match. The radio core position is coincident with the 2–10 keV peak. We also extracted the *Chandra* spectrum from a circular region of 2″ radius. The spectral parameters are not well constrained due to the poor photon statistics, but the results are in good agreement with those from *XMM–Newton*. The strong Fe K line at 6.4 keV (detected at much greater than 99% significance with *XMM–Newton*) suggests that this source is heavily absorbed and confirms the *BeppoSAX* results which indicate that it is Compton thick (Iyomoto et al. 2001).

NGC 3185 (S2:): the *XMM–Newton* observation of this object shows weak nuclear emission. An extraction radius of 20″ was chosen in order to separate the nuclear emission from a nearby ULX (Foschini et al. 2002). The spectrum is described by a power law ($\Gamma = 2.1 \pm 0.1$) with absorption lower than 2×10^{21} cm^{-2}. Radio emission is detected only marginally (HU01).

NGC 3227 (S1.5): this type 1.5 Seyfert is known to show significant spectral variability in the X-ray band (George et al. 1998) and a warm absorber (Gondoin et al. 2003). The *XMM–Newton* 0.5–10 keV spectrum is parameterized here with a single power law plus a scattered component, with the soft and hard X-ray power laws having identical slopes ($\Gamma = 1.5 \pm 0.02$, $N_{\rm H} = 6.8 \pm 0.3 \times 10^{22}$ cm^{-2}). Addition of a warm absorber would modify only slightly these continuum parameters. The Fe K line is detected at 6.4 keV with $EW = 190 \pm 40$ eV. Spectral parameters are in agreement with the best-fit results from Gondoin et al. (2003) and Lamer et al. (2003).

NGC 3486 (S2): emission from the nuclear region has been detected in the *XMM–Newton* observation, surrounded by extended emission. An extraction radius of 20″ was used in order to separate the nucleus from a nearby ULX (Foschini et al.

2002). The very poor statistics of the spectrum yield a best fit with a power law ($\Gamma = 0.9 \pm 0.2$) and Galactic absorption. The *XMM–Newton* 2–10 keV flux was measured assuming the above best-fit model, and it turns out to be consistent with the *Chandra* limit (Ho et al. 2001).

NGC 3941 (S2:): the *XMM–Newton* observation of this object shows a bright off-nuclear source 40″ from the nuclear position. The spectrum has very poor statistics and is best fitted with an unabsorbed power law with $\Gamma = 2.1 \pm 0.3$. The source is marginally detected in the radio band (HU01).

NGC 4051 (S1.5): detailed analyses of this observation have been presented by Uttley et al. (2003) and Pounds et al. (2004), and have been compared to the earlier observation performed in 2001 (Lamer et al. 2003). Major spectral variations between the high-flux and low-flux states have been interpreted either in terms of variations in the ionization state of the absorption column density (Pounds et al. 2004) or in terms of large changes in the power-law slope (Uttley et al. 2003). Here, we fitted the 0.5–10 keV integrated spectrum of the low-flux state with a soft thermal component plus a steep scattered power law, and a very flat hard power law ($\Gamma = 1.2 \pm 0.1$). The flat power-law shape, together with the strong Fe K emission line at 6.4 keV with $EW \approx 250$ eV and the two absorption edges marginally detected at 7.2 and 7.9 keV, suggest the presence of both a strong reflection component and a heavy warm absorber, in agreement with Pounds et al. (2004). Further detailed temporal analysis is beyond the scope of the present work. NGC 4051 shows complex radio structure (HU01).

NGC 4138 (S1.9): the *XMM–Newton* image of this object shows a bright nuclear source with marginal evidence of a surrounding diffuse component. Detailed imaging and spectral fitting of the same dataset is reported by Foschini et al. (2002). The best-fit model is obtained with an intrinsic absorbed power-law component ($\Gamma = 1.5 \pm 0.1$, $N_{\rm H} = (8 \pm 1) \times 10^{22}$ cm^{-2}) plus an Fe line at 6.4 keV ($EW = 83 \pm 30$ eV). We add a scattered component plus a thermal component to fit the data below 1.5 keV ($kT = 0.3 \pm 0.05$ keV, $\Gamma_{\rm SX} \equiv \Gamma_{\rm HX}$). A weak, compact radio core is seen at the position of the optical nucleus (HU01).

NGC 4151 (S1.5): EPIC images show a bright, point-like nuclear source. The spectrum below 1.5 keV is complex and can be described in terms of a warm absorber, scattered radiation, and additional spectral components (see, e.g., Yang et al. 2001; Ogle et al. 2000). We concentrate here on the 2–10 keV spectrum and obtain a good description with an absorbed power law ($\Gamma = 1.6 \pm 0.1$, $N_{\rm H} = 8.4 \pm 4 \times 10^{22}$ cm^{-2}) plus a soft scattered component with $\Gamma = 1.8 \pm 0.5$. A strong Fe K line is detected with $EW \approx 300 \pm 30$ eV and 41 ± 15 eV for the Kα and Kβ components. More detailed analysis of the same dataset is given by Schurch et al. (2004). A complex radio structure is present in this source (HU01).

NGC 4258 (S1.9): the *XMM–Newton* image of this source shows a bright, hard, point-like nucleus and unresolved diffuse emission. The *XMM–Newton* spectral results are in good agreement with those shown by Pietsch & Read (2002). The *XMM–Newton* hard spectrum is modeled by a power law ($\Gamma = 1.7 \pm 0.1$) with high absorption ($N_{\rm H} = 8.7 \pm 0.3 \times 10^{22}$ cm^{-2}). A narrow Fe Kα emission line is marginally detected ($EW = 27 \pm 20$ eV). The *XMM–Newton* hard luminosity is a factor of 2 lower than the *Chandra* luminosity (Young & Wilson 2004). This difference is probably due to intrinsic variability, already found between previous *ASCA* and *BeppoSAX* observations (Terashima et al. 2002; Risaliti 2002). The same is true for the Fe Kα line which had been detected in previous *ASCA* and *BeppoSAX* observations but which is not significantly detected here.

NGC 4388 (S1.9): the 2–10 keV *XMM–Newton* data show a bright nucleus embedded in diffuse emission extending to a radius of ∼20″ in the full-band image. An unusually high background level precludes detailed analysis of the extended component. The spectrum from the nuclear region, with the background determined locally, is well fitted by a complex (thermal plus scattered) soft component plus a hard ($\Gamma = 1.2 \pm 0.2$), heavily absorbed ($N_{\rm H} = 2.7 \times 10^{23}$ cm^{-2}), power-law component. A strong Fe Kα line at 6.4 keV is detected ($EW \approx 450 \pm 70$ eV). Our spectral results are in good agreement with those reported by Iwasawa et al. (2003).

NGC 4395 (S1.5): this source is well known for showing large amplitude, complex flux and spectral variations (see, e.g., Iwasawa et al. 2000; Shih et al. 2003; Moran et al. 2005). Detailed analysis of the *XMM–Newton* observations is given by Vaughan et al. (2005) and Iwasawa et al. (2005). For a simpler comparison with other sources, we consider here only its time-averaged properties and parameterize its spectrum with a hard power-law model ($\Gamma = 1.2$) absorbed by a column density of $N_{\rm H} \approx (5.3 \pm 0.3) \times 10^{22}$ cm^{-2}, plus a soft complex component which includes thermal emission and a scattered power law. An iron line is detected at 6.4 keV ($EW \approx 100 \pm 25$ eV). A second line is found at ∼6.2 keV, with $EW = 45 \pm 30$ eV.

NGC 4472 (S2::): this is a giant elliptical galaxy. The *XMM–Newton* image reveals strong, soft, diffuse emission. A *Chandra* 2–10 keV image (Loewenstein et al. 2001; Soldatenkov et al. 2003) shows complex structure (including diffuse and off-nuclear point sources) without any evidence for a dominant core emission. For this reason, the hard X-ray flux and luminosity are treated here as upper limits. The *XMM–Newton* spectrum is mostly thermal and poorly parameterized here by a single thermal component plus a hard power-law tail. The spectrum is shown in Appendix A, but it is not used in our analysis. This source is marginally detected in the radio band (HU01).

NGC 4477 (S2): the X-ray spectrum obtained from *XMM–Newton* is the first for this object. The EPIC images show that the nucleus seems to be dominated by diffuse soft emission. The 2–10 keV image for this source is not unambiguously compact and is very weak. The spectrum was extracted from a region of radius 25″ to separate the nuclear emission from a possible off-nuclear source at a distance of ∼40″ from the nucleus. The 0.5–10 keV spectrum appears to be dominated by the soft component ($kT = 0.4 \pm 0.1$ keV). Above

2 keV the statistics are very poor and the data can be fitted with an absorbed power law ($\Gamma = 1.9 \pm 0.3$, $N_{\rm H} \leq 2 \times 10^{22}$ cm^{-2}). This source is marginally detected in the radio band (HU01).

NGC 4501 (S2): the 2–10 keV MOS1 and MOS2 images reveal the presence of a weak nuclear core. The spectrum was extracted from a region of 20″ radius in order to exclude the emission of an off-nuclear source (Foschini et al. 2002). The 0.5–10 keV spectrum is described by a soft thermal component ($kT = 0.4 \pm 0.1$ keV) plus a power law with $\Gamma = 1.5 \pm 0.3$. Absorption in excess of the Galactic value is not required by the fit, yielding an upper limit for the column density ($N_{\rm H} \leq 2 \times 10^{21}$ cm^{-2}). This is consistent with previous *AS CA* results reported by Terashima et al. (2002). An unresolved radio core is also detected (HU01).

NGC 4565 (1.9): Mizuno et al. (1999) revealed the presence of two bright point-like sources in the *AS CA* observation of this galaxy. A *Chandra* study of NGC 4565 by Wu et al. (2002) leads to a clear identification of the nuclear source which is separated from the off-nuclear source by ∼50″. The parameters describing the *Chandra* 0.5–10 keV spectrum, with poor statistics, are in good agreement with those found by Terashima & Wilson (2003) using the same data set. Also, in the *XMM–Newton* images the two sources are clearly separated (Foschini et al. 2002). We extracted the spectrum from a region of radius 25″. We find that a power law with a low amount of absorption gives a good fit for the spectrum ($\Gamma = 1.8 \pm 0.2$, $N_{\rm H} \leq 1.2 \times 10^{21}$ cm^{-2}). The *XMM–Newton* and *Chandra* fluxes are in good agreement. The radio nucleus has been detected and it is possibly variable (HU01).

NGC 4579 (S1.5/L1.5): this object has been observed by *Chandra* for ∼35 ks (Eracleous et al. 2002) and ∼3 ks (Ho et al. 2001; Terashima & Wilson 2003). *Chandra* images show a hard compact nucleus surrounded by soft diffuse emission which extends for ∼40″ in radius. The *XMM–Newton* spectrum is best fitted with a soft thermal component ($kT \approx 0.6$ keV), a power law with $\Gamma \approx 1.8$, plus two iron Gaussian lines, one at ∼6.4 keV with $EW \approx 170 \pm 50$ eV and one at ∼6.85 keV with $EW \approx 140 \pm 60$ eV. We find no absorption in excess of the Galactic value. The *XMM–Newton* fluxes and luminosities are in good agreement with the Eracleous et al. (2002) and Ho et al. (2001) results. A radio core is detected (HU01).

NGC 4639 (S1.5): the *XMM–Newton* image shows a bright nucleus surrounded by weak diffuse emission which is less prominent in the 2–10 keV image. This is similar to what was obtained with the *Chandra* images (Ho et al. 2001), thus excluding contamination from unresolved sources. The *XMM–Newton* spectrum is well fitted by a simple power law with $\Gamma \approx 1.8$ and no absorption in excess of the Galactic value. The *XMM–Newton* observation yields a hard X-ray flux ($F_{2-10\ \rm keV} \approx 2.3 \times 10^{-12}$ erg s^{-1} cm^{-2}) about two times higher than the *AS CA* flux (Ho et al. 1999; Terashima et al. 2002). The source is marginally detected in the radio band (HU01).

NGC 4698 (S2): the X-ray nuclear region of this object has been studied in detail using *Chandra* data which reveal a few possible ULXs within NGC 4698. Two of these are as close as ∼30″ from the optical-radio nuclear position (Georgantopoulos & Zesas 2003). The *XMM–Newton* images show a weak nucleus. Its spectrum was extracted from a region of radius 25″ to exclude any possible contamination from the nearest two ULXs, which are marginally detected. The *XMM–Newton* flux is in good agreement with the *Chandra* one. A power-law fit with $\Gamma = 2.0 \pm 0.2$ gives a good fit to the *XMM–Newton* data. We measured very low intrinsic absorption ($N_{\rm H} \leq 4 \times 10^{21}$ cm^{-2}). NGC 4698 is marginally detected in the radio band (HU01).

NGC 4725 (S2:): this source has not been detected in the radio band (HU01), so we use the optical position to determine the nuclear position. The *XMM–Newton* image reveals the presence of a nuclear core and of several nearby off-nuclear sources positioned at ≳30″ from the nucleus. The spectrum was extracted with a radius of 20″ to avoid contamination from these off-nuclear sources. Despite the poor statistics, the spectrum is best fitted with two distinct components: a soft thermal component with $kT = 0.3 \pm 0.1$ keV, and a hard power-law component with $\Gamma = 1.9 \pm 0.3$ with absorption $\leq 4 \times 10^{22}$ cm^{-2}. The *XMM–Newton* hard flux is a factor of ∼2 times lower than the *Chandra* flux (Ho et al. 2001), indicating possible intrinsic variability of this object.

NGC 5033 (S1.5): despite the presence of very high background flares during the *XMM–Newton* observation, the source is clearly detected. We use an extraction radius of 20″ and a local background subtraction for the analysis. The spectrum is best modeled with a power law ($\Gamma = 1.7 \pm 0.1$), with no absorption in excess of the Galactic value. We detect an iron line at 6.4 keV (with $EW = 470 \pm 215$ eV). These results agree well with those from *ASCA* (Terashima et al. 1999, 2002). A radio core is detected (HU01).

NGC 5194 (S2): in the *XMM–Newton* images, this galaxy (also called M51) shows a complex nuclear region characterized by extended features and off-nuclear sources in the soft band, but the nucleus is compact in the hard band. This is similar to, and consistent with, what is found in the *Chandra* images by Terashima & Wilson (2001). The bright nucleus is seen in the optical position coincident with the radio core position (HU01). The soft emission has been modeled with a thermal plasma with $kT = 0.5 \pm 0.1$ keV, and the hard component with a very flat power law with photon index $\Gamma \approx 0.6$. The iron line detected at ∼6.4 keV is very strong, with $EW \approx 1$ keV, which is a clear indication of the Compton-thick nature of this source. This has also been confirmed by a *BeppoSAX* observation of M 51 which has shown that the nucleus is absorbed by a column density of 5.6×10^{24} cm^{-2} (Fukazawa et al. 2001).

NGC 5273 (S1.5): the *XMM–Newton* observation shows a bright compact nucleus in both the soft and hard energy bands. Higher angular resolution *Chandra* images reveal the presence of a compact core coincident with the radio position (HU01) and the presence of a comparatively weak off-nuclear source 20″ from the nucleus. The *XMM–Newton* spectrum is properly fit by a power-law model with $\Gamma \approx 1.5$ and an absorption column of 0.9×10^{22} cm^{-2}, plus a soft thermal component with $kT \approx 0.2$ keV, and an Fe K line at 6.4 keV with $EW = 226 \pm 75$ eV. There is also a marginal detection of an absorption edge at ∼7.8 keV, indicating the possible presence of an ionized absorber.